



**Politecnico
di Torino**

Master's Thesis in Mechanical Engineering

Optimized Control of PMSM-Quadrotor UAV System

Student:

Morteza Moslehi S301790

Supervisor:

prof. Stefano Primatesta

Co-supervisors:

prof. Giorgio Guglieri,
Ing. Marco Rinaldi

Academic year 2023-24

Abstract

Quadrotor Unmanned Aerial Vehicles (UAVs) are flying mechatronic systems equipped with propellers, motors, electronic speed controllers, and sensors integrated into their cross-shaped structure. Quadrotor UAVs are widely recognized as the most promising configuration of UAV for their controllability and relatively low cost. Among brushless motors, Permanent Magnet Synchronous Motors (PMSMs) are remarkably dependable and efficient. Without compromising the torque generation capability, PMSMs can help reduce the size of the platform thanks to their power-to-size ratio. PMSMs enhance UAV control by generating thrust and improving maneuverability. The literature rarely considers motor dynamics even though it is crucial for the development of the drone digital twin. This paper investigates the performance of a quadrotor equipped with four PMSMs, focusing on its behavior during hovering and maneuvering. Controlling UAVs with PMSMs involves controlling motors' speed to control the drone's direction, this is typically achieved with a series of decentralized Proportional-Integral-Derivative (PID) controllers. To further optimize the performance of the closed-loop system, a Particle Swarm Optimization (PSO) algorithm is designed to tune the parameters of each PID controller.

The quadrotor model is derived adopting the Newton-Euler approach and is intended to be constituted by four three-phase PMSMs controlled with a velocity control loop-based Field Oriented Control (FOC) technique. The PSO algorithm is used to tune the parameters of the PID controllers of quadrotor height, quadrotor attitude angles, and PMSMs rotational speeds which represent the eight critical parameters of the PMSM-quadrotor UAV system. The PSO algorithm is designed to optimize eight Square Error (SE) cost functions which quantify the error dynamics of the controlled variables. For each stabilization task, the PID tuning is divided in two phases. Firstly, the PSO optimizes the error dynamics of altitude and attitude angles of the quadrotor UAV. Secondly, the desired steady-state rotational speeds of the PMSMs are derived, and the PSO is used to optimize the motors dynamics. Finally, the complete PMSM quadrotor UAV system is simulated for stabilization during the target task. The study is carried out by means of simulations in MATLAB/Simulink. The validity of the approach is corroborated by extensive simulation campaigns with different initial conditions for both hovering and maneuvering tasks. By exploiting the PSO algorithm for the optimal tuning of all the PID controllers of the system it is possible to comprehensively simulate the PMSM-quadrotor UAV system and optimize the performances.

Index

1. Chapter 1.....	1
1.1 Introduction:.....	1
2. Chapter 2.....	3
2.1 State of the art.....	3
3. Chapter 3.....	5
3.1 Quadrotor Model:.....	5
3.2 System Model:.....	5
3.3 PMSM Model:.....	10
3-3-1 DESCRIPTION OF THE DRIVE SYSTEM:.....	11
3-3-2 PMSM Motor:.....	11
3.3.3 Permanent Magnet Material:.....	11
3.3.4 Classification of Permanent Magnet Motors:.....	12
3.3.5 Permanent magnet radial field motors:.....	12
3.3.6 Position Sensor:.....	13
3.3.7 Current Controlled Inverter:.....	13
3.3.8 Current Control:.....	13
3.3.9 PWM Current Controller:.....	13
3.3.10 MODELING OF PM DRIVE SYSTEM:.....	13
3.3.11 Parks Transformation and Dynamic d q Modeling:.....	15
3.3.12 PM MOTOR CONTROL:.....	16
3.3.14 Constant Torque Operation:.....	17
3.3.15 THE FLUX-WEAKENING:.....	18
3.3.16 Speed Control of PM Motor:.....	18
3.4 System Control:.....	20
3.4.1 Control law for quadrotor:.....	20
3.4.2 Modelling for Control:.....	20
3.4.3 Control model of Quadrotor:.....	21
3.4.5 Control model for PMSM:.....	22
3.4.6 PMSM Motor Model:.....	24
3.5 OPTIMIZATION METHOD.....	27
3.5.1 The conceptual framework:.....	27
3.5.2 The fundamental PSO method:.....	27

3.5.3 Algorithm:.....	28
3.5.4 FLOWCHART of PSO:.....	29
4. Chapter 4.....	30
4.1 Simulation Setting:.....	30
4.1.1: Quadrotor Simulation Setting:.....	30
4.1.1.1: PID controller block:	30
4.1.1.2: Motor model block:	31
4.1.1.3: Quadrotor Model Block:.....	31
4.2 Simulation Results:.....	32
4.2.1 Hovering:	33
4.2.2 Maneuvering:	39
Reference:	47

Nomenclature

UAVs	Unmanned Aerial Vehicles
PMSMs	Permanent Magnet Synchronous Motors
OXYZ	A stationary inertial reference frame
oxyz	A body reference frame
T_L	Homogeneous transformation matrix
RPY	Convention comprises three rotations
ψ	Euler yaw angle) about the Z axis
θ	Euler pitch angle) about the Y_1 -axis
φ	Euler roll angle) about the X_2 -axis
C	Cosine
S	Sine
T_g	Transforms rotational movement-related Vectors from the inertial frame
P, q, r	The rotational velocities within the body frame
ϕ' , ϑ' , and ψ'	The Euler rates
R	Represents the position vector in the inertial Frame
F_1	The thrust force generated by rotor
ω_i	Indicates the angular speed of rotor i,
b	The thrust coefficient
m	The mass of the quadcopter
g	Acceleration due to gravity
K	The aerodynamic thrust drag coefficient.
L	Quadrotor's arm length
I	Inertia matrix
I_R	The inertia of the rotors
d	The drag coefficient
K_d^R	Aerodynamic moment drag coefficient
M	Rotors' induced moment vector
M_{gy}	The gyroscopic moment vector
U_1	The overall lift force generated by the rotors
U_2, U_3	The forces that induce pitch and roll movements
U_4	The moment that influences the yaw axis
v_d, v_q	The dq-axis voltages
i_d, i_q	The dq-axis currents
R_s	The stator resistance
L_d, L_q	The dq-axis inductances
ω_r	The rotor angular velocity (electrical rad/s)
λ_f	The flux linkage due to the permanent magnet
J	The rotor inertia
T_e	The electromagnetic torque

T_L	The load torque
B	The viscous friction coefficient
K_p	The proportional gain
K_i	The integral gain
K_d	The derivative loop
K_{pd}, K_{id}, K_{dd}	The proportional, integral and derivative gains for the d-axis current
K_{pq}, K_{iq}, K_{dq}	The proportional, integral and derivative gains for the q-axis current controller
ω_{pso}	Inertia weight of pso

List of Figures

Figure1. Quadrotor Model Illustration [39]	5
Figure2: Quadrotor Configuration Layout [11]	7
Figure3. PMSM Model Illustration, taken from [39].....	10
Figure 4. Schematic Representation of PMSM Control	11
Figure 5. Surface Permanent Magnet Motor [40]	12
Figure 6. d-q Model in PMSM [39]	14
Figure 7. Constant Torque and Flux-Weakening Treatment [39].....	16
Figure 8. PMSM Motor Design	19
Figure 9. Illustration of PID Controller	19
Figure 10. Flow Chart of PSO [40].....	29
Figure 11. Complete model.....	30
Figure 12: PID Controller model	30
Figure 13. Motor model	31
Figure 14: The Permanent Magnet Synchronous Machine Model	31
Figure 15. Complete model of quadrotor.....	32
Figure 16: non-optimization results for Hovering	34
Figure 17: optimized result of Hovering.....	35
Figure 18: Comparing optimize and non-optimize control of PID in Hovering.....	36
Figure19: Result of the Controlled Rotational Speed	37
Figure 20: Complete Result of Controlled UAVs in Hovering	37
Figure 20: Non-optimized Results of Random Initial Parameters for Hovering Controller.....	38
Figure 21: Optimized Results of Random Initial Parameters for Hovering Controller.	39
Figure 22. Non-Optimization Results for Maneuvering	40
Figure 23: optimized result of Maneuvering.....	41
Figure 24: Comparing Optimized and Non-Optimized PID Control for Maneuvering.....	42
Figure25: Result of the Controlled Rotational Speed for Motors 1,3	43
Figure 26: Result of the Controlled Rotational Speed for Motors 2,4.....	43
Figure 27: Complete Result of Controlled UAVs in Maneuvering	44
Figure 28: Non-optimized Results of Random Initial Parameters for Maneuvering Controller	45
Figure 29: Optimized Results of Random Initial Parameters for Maneuvering Controller.....	46

1. Chapter 1

1.1 Introduction:

Unmanned Aerial Vehicles (UAVs) are recent devices created by humans to enhance feasibility in various fields. UAVs are equipped with a specific number of propellers, motors, electronic speed controllers (ESCs), and sensors, all of which are mounted on the frame or structure. The UAVs or drones are being utilized due to their special characteristics such as speed, agility, and ability to access dangerous locations without harming humans. They are commonly used in agriculture, photography, videography, search and rescue operations, and have recently been implemented by delivery companies.

One of the important roles of drones could be mentioned in search and rescue missions. This type of vehicle, equipped with special cameras and sensors, is used not only for investigating specific areas but also for helping identify missing persons, survivors, or hazards and accessing places that humans are unable to reach.

With the increasing demand for internet shopping and fast delivery, retailers and grocery chains are turning to last-mile delivery drones. These flying vehicles make deliveries from nearby retailers or warehouses, offering a more efficient alternative to traditional delivery methods [1-3]. Major corporations like Amazon, Walmart, Google, FedEx, UPS, and others are actively testing different types of delivery drones to streamline their delivery processes. The goal is to provide customers with quick and convenient delivery options in an increasingly competitive market.

Drones with LiDAR technology is used to make 3D modelling easier. These drones have LiDAR sensors installed, which allow them to collect detailed data while scanning terrain in order to create 3D models. LiDAR-equipped drones can provide noticeably more accurate data. LiDAR not only helps drones navigate on different types of terrain, but it also helps them identify targets for search and rescue operations, evaluate crops, and perform other functions.

Brushless Permanent Magnet Synchronous Motors (PMSMs) are incredibly dependable and efficient. They have a reduced frame size, no rotor current, and more torque due to their permanent magnet rotor. Without compromising torque, PMSMs can help to reduce the size of your design due to their outstanding power-to-size ratio. It has been widely applied in electric vehicles, robots, servo systems, and aerospace applications due to its simple design, compact structure, and high energy density. Given its function and benefits, PMSM motors are quite helpful for rotating UAV propellers.

Controlling UAVs using PMSM motors involves utilizing the motor's speed and torque characteristics to maneuver the drone in the desired direction, a task typically accomplished through the use of a PID controller. The PMSM motor plays a role in controlling UAVs through thrust generation, flight stability, maneuverability, and autonomy.

In this thesis, the quadrotor control simulation was performed using MATLAB and Simulink. The control system was evaluated during different phases, including hovering and maneuvering, using specific input parameters. A PID controller was used, and its parameters were optimized with the PSO algorithm.

Subsequently, the four PMSM motors were simulated to achieve the necessary rotational speeds for these phases, with further optimization of the PID parameters by PSO. In the final stage, the entire quadrotor and PMSM motors were simulated to showcase their capabilities in various missions

2. Chapter 2

2.1 State of the art

Dr. Cooper and Elmer Sperry created the automatic gyroscopic stabilizer, which aids in maintaining an aircraft's level and straight flight path, a few years after the first manned airplane flight. This technology was utilized to create the first radio-controlled Unmanned Aerial Vehicle (UAV) from a U.S. Navy Curtiss N-9 trainer aircraft. categorizes pilotless aircraft into three groups: Unmanned Aerial Vehicles (UAV), Remotely Piloted Vehicles (RPV) and Drone [4]. The primary factors that distinguish the various categories are the purpose of the mission, the size, the flying envelope, and—above all—the degree of operational autonomy. RPVs, for example, are not the same as UAVs in that UAVs can function independently of a remote controller, whereas RPVs, as their name suggests, are guided and controlled from a ground station. Unmanned aerial vehicles (UAVs) can be broadly categorized into two groups: autonomous aircraft and autonomous helicopters [5]. A quadcopter is a helicopter with four propellers. Two sets of counterrotating rotors are located at either end of a symmetric cross-frame, which is centered around the origin of the reference system utilized, to form the quadcopter. By altering the rotational speeds of each of the four rotors, a quadcopter's fundamental motions can be recreated by adjusting the lift (or thrust) forces, both absolute and differential. The helicopters have clear advantages over the aero planes due to their specific capabilities like better hovering operation, ability of landing/take-off in limited space, etc. There is a significant number of publications describing the mathematical modelling, These trajectory tracking control methods mainly study how to reduce the trajectory tracking error with small consumption [6]. Two methods are used to model quadrotors: Newton-Euler [7-9] and Euler-Lagrange [5, 9, 10]. In both methods, a quadrotor aerial robot can achieve 6 degrees of freedom (DOF) movement in the inertial frame by adjusting the rotational speed of its motors. These six degrees of freedom encompass three translational motions along the coordinate axes and three rotational motions around the rotary axes (roll, pitch, and yaw). A. Taame et al. [11] studied methods to use the Euler-Lagrange formalism to achieve the dynamic modeling of a quadcopter drone. The primary goal of developing a cascade control strategy using the backstepping approach was to guide the quadcopter in both altitude and attitude to ensure trajectory. The Euler-Lagrange approach was used by Keyur Patel and Jayesh Barve [12] to define the equation of motion while accounting for small adjustments to allow for fluctuating air density. Via simulations of customized models, they compared popular control methods as PD, PID, and back-stepping control. Yasmina BESTAOUI and Hervé KUHLMANN [13] presented the preliminary results of a model of a quadrotor airship, considering the effects of wind as well as the varying mass effects, using the Newton formulation. M. Rinaldi et al. [14] presented a nonlinear dynamical model for a quadrotor UAV developed using the Newton-Euler method, alongside a proposed control architecture for 3D trajectory tracking.

Permanent magnet motors are an ideal option for specific uses like aircraft, marine vessels, and electric vehicles such as UAVs due to their ability to withstand faults and their high-power density. A review of earlier studies on d-axis and q-axis inductance identification strategies for permanent magnet synchronous motors (PMSM) is offered, along with an explanation of the various parameter identification methods provided in [15, 16]. R. Sadou et.al, [17] presents a novel approach to optimize the geometry, control schemes, and computational efficiency of Permanent Magnet Synchronous Motors (PMSM) for Unmanned Aerial Vehicles (UAVs) in order to reduce weight and losses while taking torque and propeller rotational speed into account. In order to examine the impact of machine dynamic performance on the aircraft's motion route from takeoff to constant level flight, Olusegun Solomon and Parviz Famouri [18] investigated the link between aircraft motion equations and machine equations. In order to direct a quadrotor towards achieving its intended mission, the development of a control system is imperative. This system encompasses positional regulation for linear movement and attitude adjustment for rotational movement [19]. Literature

reviews, exemplified by sources [20-23] offer an exhaustive examination of the primary cutting-edge control tactics employed for quadrotor UAVs.

The Proportional-Integral-Derivative (PID) controller holds a significant historical legacy in the field of automatic control. Its origins trace back to James Watt's development of the steam engine and governor in 1769, recognized as the first instance of a negative feedback device. In 1868, J. C. Maxwell further advanced this concept by formulating a mathematical model for the governor control of the steam engine. [24-26]. In process industries, less sophisticated proportional-integral-derivative (PID) controls are still widely used. PID controllers' long-lasting popularity can be linked to their straightforward control structure, easy implementation that makes use of operators' experience, and unambiguous understanding of the physical importance of control parameters. But even with these benefits, there are restrictions when it comes to creating PID controllers. Because most process systems are inherently nonlinear, it can be difficult to achieve adequate control performance with fixed PID parameters alone [27]. Ivan Lopez-Sanchez and Javier Moreno-Valenzuela [28] conducted a study that explores the implementation of PID control configurations in quadrotor UAVs, with particular attention to a range of approaches encompassing linear, nonlinear, discontinuous, fractional-order, intelligent, and adaptive schemes. Zhih et al [29] developed an autopilot for quadrotor UAVs based on PID control.

Control Lyapunov function (CLF) is a successful attempt to directly use of the Lyapunov function stability analysis technique of nonlinear systems in the synthesis problem [30]. In control systems, sliding mode control (SMC) is a nonlinear control technique that modifies the behavior of a nonlinear system through the application of a discontinuous control signal (or more precisely, a set-valued control signal), compelling the system to "slide" across a section of its typical behavior. Xue-ying Jiang et al. [31] presented an adaptive backstepping sliding mode solution for quadrotor UAV flight attitude is proposed to solve nonlinear and 6-DOF (degrees of freedom) under-actuated difficulties for the attitude and position of the drones. Furthermore, by applying Lyapunov theory, it is demonstrated that the tracking error of the design method asymptotically converges to zero. The survey covers controlling strategies in PMSM and current research trends in the field. Additionally, it identifies research gaps and presents a futuristic line of inquiry [32]. Ullah, Ket.al [33] presented an overview of the many robust control techniques that are suitable for PMSMs and assesses how well a speed controller is being implemented.

Optimization methods are utilized across various fields of study to seek solutions that either maximize or minimize certain parameters, such as minimizing production costs, maximizing profits, reducing raw material usage in product development, or maximizing production output [34]. A literature review on UAVs and the implementation of optimization methods has been published [35-37]. The population-based stochastic optimization algorithm known as particle swarm optimization (PSO) is inspired by the clever group behavior of certain animals, such as fish schools or flocks of birds. It has undergone numerous improvements since it was first introduced in 1995 [38]. Qingbo Geng and Zheng Zhao [39] study the basic model of UAV track planning, apply the basic Particle Swarm Optimization (PSO) algorithm, and propose an improved hybrid particle swarm UAV route planning method with a contraction factor to demonstrate its simplicity, effectiveness, and ability to meet the requirements of UAV path planning. The genetic method is a robust optimization algorithm that is designed to reliably locate a global optimum even in the presence of local optima. A genetic algorithm (GA)-based preliminary design optimization methodology for unmanned aerial vehicles (UAVs) is presented by Vivek Ahuja and Roy J. Hartfield [40]. Vincent Roberge et al. [41] compared the Particle Swarm Optimization (PSO) and Genetic Algorithm (GA) in order to solve the challenge of determining viable and nearly-optimal trajectories for fixed-wing UAVs in a complex three-dimensional environment while taking the vehicle's dynamic characteristics into consideration.

3. Chapter 3

3.1 Quadrotor Model:

Quadrotor Unmanned Aerial Vehicles (UAVs) are mechanical-electronic systems featuring two solid arms set in a cross shape, alongside four rotors, as shown in figure1. These rotors, positioned at the ends of each



Figure1. Quadrotor Model Illustration

arm, spin in opposite directions. The velocity of each rotor is managed separately. The motion of quadrotors could be divided into two motions, linear motion of mass center and rotational motion around the center of mass. Therefore, to describe the motion in space in each second, we need a 6 degree of freedom. 3 degrees could be utilized for axes x , y , z and rest for rotational motion, roll φ , pitch θ , yaw ψ . The control of these 6 degrees of freedom is done by tuning the velocity of rotational of these rotors.

3.2 System Model:

The flight maneuverability of quadrotors results from the combined lift generated by all rotors and their ability to tilt. This tilting capability arises from the forces acting on the arms and the counter-torque generated by pairs of rotors. Two reference frames are established to describe the position and orientation of the UAV: a stationary inertial reference frame denoted as $OXYZ$ and a body reference frame $oxyz$ affixed to the quadrotor. The relationship between these frames is articulated through the homogeneous transformation matrix T_l , derived using the Euler ZYX convention, also recognized as the RPY convention. The RPY convention comprises three rotations. Initially, a rotation of ψ (Euler yaw angle) about the Z -axis generates the frame OX_1Y_1Z . Subsequently, a second rotation of θ (Euler pitch angle) about the Y_1 -axis yields the frame $OX_1Y_1Z_1$. Finally, a third rotation of φ (Euler roll angle) about the X_2 -axis results in the frame $OX_2Y_2Z_2$, coinciding with the body frame $oxyz$.

$$\begin{aligned}
T_\varphi &= \begin{bmatrix} 1 & 0 & 0 \\ 0 & c\varphi & -s\varphi \\ 0 & s\varphi & c\varphi \end{bmatrix} \varphi \in (-\pi, \pi) \\
T_\theta &= \begin{bmatrix} c\theta & 0 & s\theta \\ 0 & 1 & 0 \\ -s\theta & 0 & c\theta \end{bmatrix} \theta \in \left(-\frac{\pi}{2}, \frac{\pi}{2}\right) \\
T_\psi &= \begin{bmatrix} c\psi & -s\psi & 0 \\ s\psi & c\psi & 0 \\ 0 & 0 & 1 \end{bmatrix} \psi \in (-\pi, \pi)
\end{aligned} \tag{1}$$

These rotations adhere to a post-multiplication rule:

$$\begin{aligned}
T_L &= T_\psi \cdot T_\theta \cdot T_\varphi \\
T_L &= \begin{bmatrix} c\theta c\psi & s\varphi s\theta c\psi - c\varphi s\psi & c\varphi s\theta c\psi + s\varphi s\psi \\ c\theta s\psi & s\varphi s\theta s\psi + c\varphi c\psi & c\varphi s\theta s\psi - s\varphi c\psi \\ -s\theta & s\varphi c\theta & c\varphi c\theta \end{bmatrix}
\end{aligned} \tag{2}$$

Where, "c" and "s" represent the cosine and sine functions, respectively. The transformation matrix T_L converts linear movement-related vectors from the body frame $oxyz$ to the inertial frame $OXYZ$. Conversely, T_g transforms rotational movement-related vectors from the inertial frame $OXYZ$ to the body frame $oxyz$.

$$\Delta = \begin{pmatrix} p \\ q \\ r \end{pmatrix} = T_\varphi^T \begin{pmatrix} \varphi' \\ 0 \\ 0 \end{pmatrix} + T_\varphi^T T_\theta^T \begin{pmatrix} 0 \\ \theta' \\ 0 \end{pmatrix} + T_\varphi^T T_\theta^T T_\psi^T \begin{pmatrix} 0 \\ 0 \\ \psi' \end{pmatrix} = T_R \begin{pmatrix} \varphi' \\ \theta' \\ \psi' \end{pmatrix} \tag{3}$$

Where, p, q, and r represent the rotational velocities within the body frame, whereas φ' , θ' , and ψ' denote the Euler rates. The dynamics of the quadrotor model are described using the Newton-Euler formalism.

In the adopted model, the following assumptions are made:

- The structure is perfectly symmetrical.
- The structure is perfectly rigid.
- The quadrotor's center of mass coincides with the origin of the body fixed frame.
- The rotors' motors dynamics are neglected.
- Complex phenomena of difficult modeling are neglected, such as the ground effect, blade flapping and any other minor aerodynamical or inertial contributions not explicitly taken into account.

It follows the translational dynamical model in the inertial fixed reference frame:

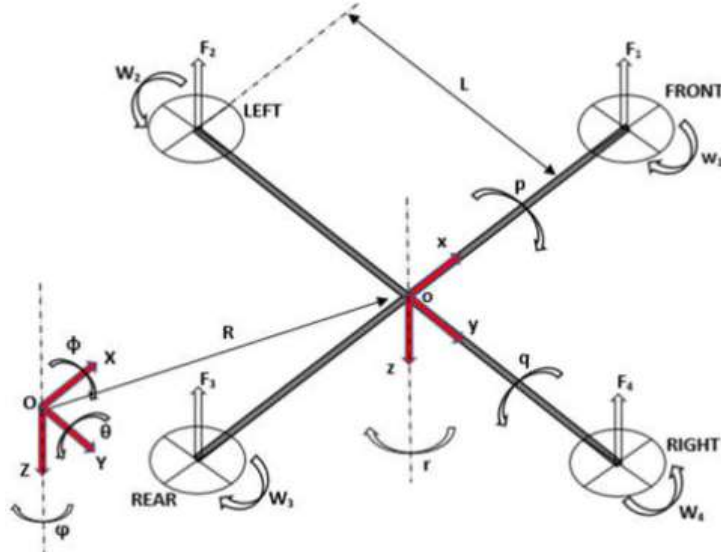


Figure2: Quadrotor Configuration Layout [11]

$$mR'' = mg - K_d^L R' - (F_1 + F_2 + F_3 + F_4) T_L \quad (4)$$

Where:

$$F_i = \begin{pmatrix} 0 \\ 0 \\ b\omega_i^2 \end{pmatrix} \quad \text{with } i=1,2,3,4 \quad (5)$$

Where, R represents the position vector in the inertial frame $OXYZ$, F_i stands for the thrust force generated by rotor i , ω_i indicates the angular speed of rotor i , b is the thrust coefficient, m denotes the mass of the quadcopter, g represents the acceleration due to gravity, and K signifies the aerodynamic thrust drag coefficient. Subsequently, the rotational dynamical model in the body reference frame ensues.

$$I\Delta' = -(\Delta \times I\Delta) - M_{gy} - K_d^R \Delta + M \quad (6)$$

Where M_{gy} is Defined as:

$$M_{gy} = I_R (\omega_1 - \omega_2 + \omega_3 - \omega_4) \Delta \times \begin{pmatrix} 0 \\ 0 \\ 1 \end{pmatrix} \quad (7)$$

Moreover,

$$M = \begin{pmatrix} L(F_2 - F_4) \\ L(F_1 - F_3) \\ d(\omega_1^2 - \omega_2^2 + \omega_3^2 - \omega_4^2) \end{pmatrix} \quad (8)$$

And

$$I = \begin{pmatrix} I_x & 0 & 0 \\ 0 & I_y & 0 \\ 0 & 0 & I_z \end{pmatrix} \quad (9)$$

Given the quadrotor's arm length denoted as L , the diagonal inertia matrix as I , the inertia of the rotors as I_R , the drag coefficient as d , the aerodynamic moment drag coefficient as K_d^R , the rotors' induced moment vector as M , and the gyroscopic moment vector as M_{gy} , the latter arising from the rotation of the propellers' axes attached to the quadrotor. The comprehensive nonlinear dynamical model of the quadrotor is obtained by assessing Equations (3) and (5) while accounting for the transformations outlined in Equations (1) and (2):

$$\begin{aligned} X'' &= -\frac{1}{m} K_d^L X' - \frac{1}{m} (s_\psi s_\varphi + c_\psi s_\theta c_\varphi) U_1 \\ Y'' &= -\frac{1}{m} K_d^L Y' - \frac{1}{m} (s_\theta s_\psi c_\varphi - s_\varphi c_\psi) U_1 \\ Z'' &= g - \frac{1}{m} K_d^L Z' - \frac{1}{m} c_\theta c_\varphi U_1 \\ p' &= \frac{I_y - I_z}{I_x} qr - \frac{I_R}{I_x} q (\omega_1 + \omega_3 - \omega_2 - \omega_4) - \frac{1}{I_x} K_d^R p + \frac{1}{I_x} L U_2 \\ q' &= \frac{I_z - I_x}{I_y} pr - \frac{I_R}{I_y} p (\omega_1 + \omega_3 - \omega_2 - \omega_4) - \frac{1}{I_y} K_d^R q + \frac{1}{I_y} L U_3 \\ r' &= \frac{I_x - I_y}{I_z} pq - \frac{1}{I_z} K_d^R r + \frac{1}{I_z} U_4 \\ \dot{\varphi} &= p + s_\varphi s_\theta c_\theta^{-1} q + c_\varphi s_\theta c_\theta^{-1} r \\ \dot{\theta} &= c_\varphi q - s_\varphi r \\ \dot{\psi} &= s_\varphi c_\theta^{-1} q + c_\varphi^{-1} c_\theta r \end{aligned} \quad (10)$$

And

$$u = \begin{pmatrix} u_1 \\ u_2 \\ u_3 \\ u_4 \end{pmatrix} = M_{bd} \omega^2 = \begin{pmatrix} b & b & b & b \\ 0 & b & 0 & -b \\ b & 0 & -b & 0 \\ d & -d & d & -d \end{pmatrix} \begin{pmatrix} \omega_1^2 \\ \omega_2^2 \\ \omega_3^2 \\ \omega_4^2 \end{pmatrix} \quad (11)$$

represents an artificial input transformation designed to simplify representation and the definition of control laws. U_1 signifies the overall lift force generated by the rotors, while U_2 and U_3 correspond to the forces that induce pitch and roll movements, respectively. U_4 represents the moment that influences the yaw axis. The described quadrotor dynamic model includes 4 state variables $x = (x_1, x_2, x_3, x_4) = (Z, \varphi, \theta, \psi)$ and 4

inputs variables $u = (u_1, u_2, u_3, u_4) = (U_1, U_2, U_3, U_4)$, Note that the rotor velocities contributing to the gyroscopic effect are still present in Equation (10). However, they can be re-expressed as a nonlinear function of the artificial input variables, $f(u)$, by inverting and manipulating Equation (11).

$$f(u) = \sum_{i=1}^4 (-1)^{i+1} \sqrt{|(M_{bd}^{-1}u)_i|} = \omega_1 + \omega_3 - \omega_2 - \omega_4 \quad (12)$$

The system, in addition to its under-actuation characteristics that inherently complicate control design, is highly nonlinear and coupled. For a dynamical system with these properties, deriving a linearized model is useful to better understand the relationship between control and state variables and to assess the system's stability. Moreover, linearized models are frequently used in the design of control laws:

$$\begin{aligned} X'' &= -\theta g \\ Y'' &= -\varphi g \\ Z'' &= g - \frac{1}{m}U_1 \\ \varphi'' &= \frac{1}{I_x}LU_2 \\ \theta'' &= \frac{1}{I_y}LU_3 \\ \psi'' &= \frac{1}{I_z}U_4 \end{aligned} \quad (13)$$

Equation (13) pertain to the linearization of the model depicted in Equation (10). This is achieved using a first-order Taylor expansion and making approximations for small angles, based on the following assumptions:

- The quadrotor is hovering: external forces and moments are negligible, and both linear and rotational velocities are small (the Euler rates match the rotational velocities in the body frame).
- The equilibrium control input and state vectors are $(u_1, u_2, u_3, u_4) = (mg, 0, 0, 0)$ and $(x_1, x_2, x_3, x_4) = (0, 0, 0, 0)$, respectively.
- All higher-order terms are neglected.

3.3 PMSM Model:

Permanent Magnet Synchronous Motors (PMSM) as shown in figure3. belong to the category of electric motors employing permanent magnets to create the necessary magnetic field for functioning. In contrast to



Figure3. PMSM Model Illustration, taken from [39]

other motor variants dependent on electromagnets, PMSMs feature magnets integrated into the rotor, thereby negating the requirement for external power to establish the magnetic field. Moreover, the advantages and disadvantages of this kind of motor could be mentioned as follows:

Advantages of PMSM:

- High efficiency: PMSMs use energy more efficiently than many other types of motors.
- Compact design: They offer a high power-to-size ratio, making them ideal for applications where space is limited.
- Precise control: PMSMs allow for accurate control over speed and torque, suitable for applications requiring precision.
- Low maintenance: With fewer moving parts and no brushes, PMSMs require minimal upkeep.
- Reduced size: Their design eliminates the need for external field windings, resulting in a more compact motor.

Disadvantages of PMSM:

- Higher initial cost: PMSMs can be more expensive to purchase initially, especially those using rare-earth magnets.
- Sensitivity to temperature: Performance can be affected by temperature changes, necessitating additional cooling measures.
- Complexity in design and control: Developing and maintaining PMSMs may require specialized knowledge and expertise.
- Limited speed range: PMSMs may have constraints in their speed range, affecting their suitability for certain applications.

- Risk of magnet demagnetization: In harsh conditions, there's a chance of permanent magnet weakening, which can degrade motor performance.

In this project involves creating a simulation for a field-oriented controlled PM motor drive system using Simulink. The simulation circuit will encompass all authentic components of the drive system, allowing for the computation of currents and voltages across various segments of the inverter and motor, both during transient and steady states. By determining losses across different sections, it aids in the inverter's design process. A closed-loop control system incorporating a PID controller within the speed loop has been engineered to function across constant torque and flux weakening regions. This system has been implemented using Simulink.

3-3-1 DESCRIPTION OF THE DRIVE SYSTEM:

The motor drive consists of four main components, the PM motor, inverter, control unit and the position sensor

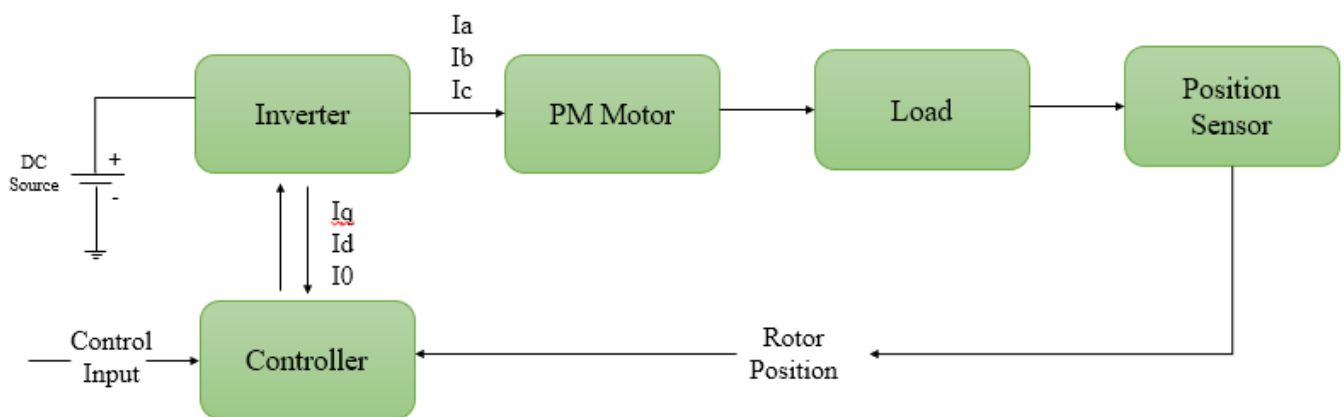


Figure 4. Schematic Representation of PMSM Control

3-3-2 PMSM Motor:

As mentioned in figure 4, permanent magnet synchronous motor (PMSM) is a motor that uses permanent magnets to produce the air gap magnetic field rather than using electromagnets.

3.3.3 Permanent Magnet Material:

The performance of the motor will be directly impacted by the permanent magnet material's qualities, therefore choosing the right material and comprehending PM motors demand appropriate knowledge. Steel that has been hardened was one of the first magnet materials produced. Steel-based magnets were readily magnetized. They were easily demagnetized, though, and had a relatively low energy capacity. Other magnet materials have been developed and used to create permanent magnets in recent years. These materials include Aluminum Nickel and Cobalt Alloys (ALNICO), Strontium Ferrite or Barium Ferrite (Ferrite), Samarium Cobalt (First-Generation Rare-Earth Magnet) (SmCo), and Neodymium Iron-Boron (Second-Generation Rare-Earth Magnet) (NdFeB). Two classes of rare earth magnets are distinguished: Neodymium Iron Boride (NdFeB) magnets and Samarium Cobalt (SmCo) magnets. Higher flux density levels are achieved by SmCo magnets, but their cost is significant. These days, NdFeB magnets are the most widely utilized rare earth magnets in motors.

3.3.4 Classification of Permanent Magnet Motors:

3.3.4.1 Direction of field flux:

The direction of the field flux is used to categorize PM motors. A radial field motor is the first classification of field flux, meaning that the flux runs along the motor's radius. The flux in the second is perpendicular to the motor's radius since it is an axial field motor. The most widely used field flux in motors is radial, although axial field flux is now being studied and utilized in a few specific applications.

3.3.4.2 Flux density distribution:

PM motors are classified on the basis of the flux density distribution and the shape of current excitation. The PMSM is designed to produce sinusoidal back EMF waves and has a sinusoidal back EMF shape. They have the following:

- Sinusoidal magnet flux distribution in the air gap
- Waveforms of sinusoidal current
- The stator conductor distribution is sinusoidal.

3.3.5 Permanent magnet radial field motors:

There are a few two possible locations for the magnets on the rotor of PM motors. They are referred to as inside permanent magnet motors or surface permanent magnet motors, depending on where they are placed. Surface-mounted PM motors feature a rotor with permanent magnets attached directly to its surface. This design simplifies construction, and specially skewed poles can be easily magnetized to reduce cogging torque. However, these motors are primarily suitable for low-speed applications due to a limitation where the magnets might separate at high speeds. Additionally, these motors are characterized by having minimal saliency, resulting in practically equal inductances in both axes. The permeability of the permanent magnet is almost that of the air, thus the magnetic material becoming an extension of the air gap. For a surface permanent magnet motor $L_d = L_q$. For simplicity in production, the rotor is made out of either punched laminations or a solid iron core. Adhesives are used to attach thin permanent magnets to the surface of the core. These magnets produce radially directed flux density over the air gap by alternating in the direction of magnetization. Torque is produced by the interaction of this flux density with currents in windings situated within slots on the inner surface of the stator.

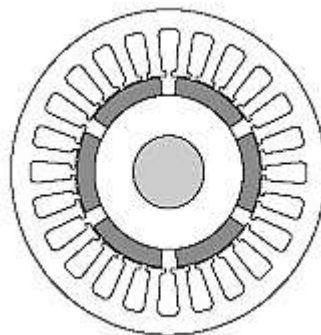


Figure 5. Surface Permanent Magnet Motor [42]

Interior PM motors feature a rotor with permanent magnets mounted internally, as illustrated in Figure 5. Each magnet is positioned within the rotor itself. While less prevalent than surface-mounted types, this configuration is well-suited for high-speed operations. However, there is inductance fluctuation due to the

permanent magnet segment acting similarly to air in magnetic circuit calculations. These motors are recognized for their saliency, with the q-axis inductance exceeding that of the d-axis $L_q > L_d$.

3.3.6 Position Sensor:

Permanent magnet synchronous motors require position sensors in the rotor shaft when operated without a damper winding. To determine rotor position, devices like potentiometers, linear variable differential transformers, optical encoders, and resolvers are used. Encoders and resolvers are most commonly employed for motors, chosen based on the desired motor performance and application requirements.

3.3.7 Current Controlled Inverter:

The motor is fed from a voltage source inverter with current control. The control is performed by regulating the flow of current through the stator of the motor. Current controllers are used to generate gate signals for the inverter. Proper selection of the inverter devices and control technique ensures the efficacy of the drive.

3.3.8 Current Control:

The power converter in a high-performance motor drive, used in motion control, essentially operates as a power amplifier. It reproduces low-power control signals generated by the field orientation controller at power levels suitable for the driven machine. High-performance drives employ control strategies to generate command signals for AC machine currents. The fundamental reason for selecting current as the controlled variable is the same as for DC machines. Current controllers can be classified into two groups: hysteresis and PWM current controllers, with PWM being utilized in this project.

3.3.9 PWM Current Controller:

PWM current controllers are widely used, with the switching frequency usually kept constant. They operate based on the principle of comparing a triangular carrier wave of desired switching frequency with the error of the controlled signal. This error signal results from the sum of the reference signal generated in the controller and the negative of the actual motor current. The comparison yields a voltage control signal sent to the gates of the voltage source inverter to produce the desired output. Its control adjusts according to the error: if the error command exceeds the triangular waveform, the inverter leg remains switched to the positive polarity (upper switch on), while if the error command is lower than the triangular waveform, the inverter leg switches to the negative polarity (lower switch on). The inverter leg is compelled to switch at the frequency of the triangular wave, producing an output voltage proportional to the current error command. The controlled output current is characterized by a reproduction of the reference current with high-frequency PWM ripple superimposed.

3.3.10 MODELING OF PM DRIVE SYSTEM:

The detailed modeling of a permanent magnet synchronous motor is presented, including discussions on field-oriented control in constant torque and flux-weakening regions. Additionally, closed-loop control of the motor is developed, employing a PID controller in the speed loop, with the design of the speed controller being discussed.

3.3.10.1 Detailed Modeling of PMSM:

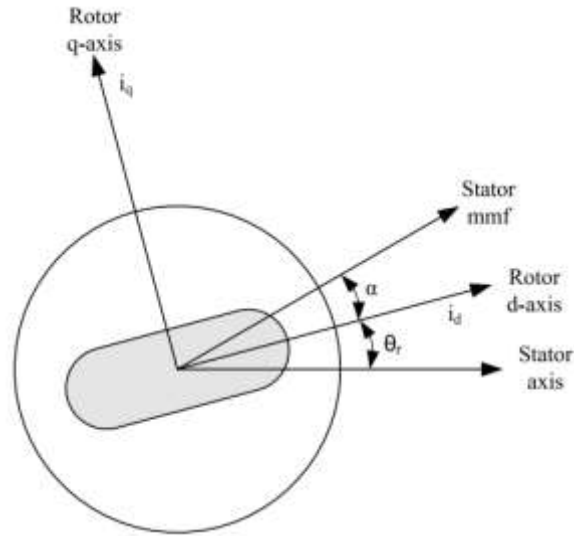


Figure 6. d-q Model in PMSM [42]

Detailed modeling of the PM motor drive system is necessary for accurate simulation. The d-q model has been developed on the rotor reference frame, as depicted in Figure 6. At any time, t , the rotating rotor d-axis forms an angle θ_r with the fixed stator phase axis, while the rotating stator mmf forms an angle α with the rotor d-axis. The stator mmf rotates at the same speed as the rotor. The PMSM model without a damper winding has been constructed on the rotor reference frame, incorporating the following assumptions:

- Saturation effects are disregarded.
- The induced EMF follows a sinusoidal pattern.
- Eddy currents and hysteresis losses are considered negligible.
- There are no dynamics associated with field current.

The voltage equations are as follows:

$$V_q = R_s i_q + \omega_r \lambda_d + \rho \lambda_q \quad (14)$$

$$V_d = R_s i_d - \omega_r \lambda_q + \rho \lambda_d \quad (15)$$

And flux linkage is defined as:

$$\lambda_q = L_q i_q \quad (16)$$

$$\lambda_d = L_d i_d + \lambda_f \quad (17)$$

Substituting equations 16-17 into 14-15 we have:

$$V_q = R_s i_q + \omega_r (L_d i_d + \lambda_f) + \rho L_q i_q \quad (18)$$

$$V_d = R_s i_d - \omega_r L_q i_q + \rho (L_d i_d + \lambda_f) \quad (19)$$

Therefore, in the matrix form we have:

$$\begin{pmatrix} V_q \\ V_d \end{pmatrix} = \begin{pmatrix} R_s + \rho L_q & \omega_r L_d \\ -\omega_r L_q & R_s + \rho L_d \end{pmatrix} \begin{pmatrix} i_q \\ i_d \end{pmatrix} + \begin{pmatrix} \omega_r \lambda_f \\ \rho \lambda_f \end{pmatrix} \quad (20)$$

The developed torque motor is being acquired by

$$T_e = \frac{3}{2} \left(\frac{P}{2} \right) (\lambda_d i_q - \lambda_q i_d) \quad (21)$$

The mechanical torque also is defined as:

$$T_e = T_L + B\omega_m + J \frac{d\omega_m}{dt} \quad (22)$$

Solving for the rotor mechanical speed form equation (22):

$$\omega_m = \int \left(\frac{T_e - T_L - B\omega_m}{J} \right) dt \quad (23)$$

And

$$\omega_m = \omega_r \left(\frac{2}{P} \right) \quad (24)$$

In the equation 11, the ω_r is the rotor electrical speed and ω_m is the rotor mechanical speed.

3.3.11 Parks Transformation and Dynamic d q Modeling:

The dynamic dq modeling technique is employed to analyze motors during both temporary changes and stable conditions. This process involves transforming the three-phase voltages and currents into dq0 variables using the Parks transformation. Transforming the phase voltage variables i_{abc} to i_{dq0} variables in the rotor reference frame yields the following eloquently derived equations.

$$\begin{bmatrix} i_q \\ i_d \\ i_0 \end{bmatrix} = \frac{2}{3} \begin{bmatrix} \cos \theta_r & \cos(\theta_r - 120) & \cos(\theta_r + 120) \\ \sin \theta_r & \sin(\theta_r - 120) & \sin(\theta_r + 120) \\ 1/2 & 1/2 & 1/2 \end{bmatrix} \begin{bmatrix} i_a \\ i_b \\ i_c \end{bmatrix} \quad (25)$$

And in order to convert from i_{dq0} to i_{abc} we have:

$$\begin{bmatrix} i_a \\ i_b \\ i_c \end{bmatrix} = \begin{bmatrix} \cos \theta_r & \sin \theta_r & 1 \\ \cos(\theta_r - 120) & \sin(\theta_r - 120) & 1 \\ \cos(\theta_r + 120) & \sin(\theta_r + 120) & 1 \end{bmatrix} \begin{bmatrix} i_q \\ i_d \\ i_0 \end{bmatrix} \quad (26)$$

3.3.12 PM MOTOR CONTROL:

Field oriented control is utilized to manage permanent magnet (PM) motors, effectively enabling synchronous motor operation akin to a DC motor. The motor's stator windings receive power from an inverter capable of producing a variable frequency and voltage output. Rather than regulating the inverter frequency autonomously, control over the frequency and phase of the output wave is achieved through a position sensor, as illustrated in fig.4. Field oriented control illustrates that an induction motor or synchronous motor can be regulated akin to a separately excited DC motor by aligning the stator mmf or current vector with respect to the rotor flux to achieve a desired outcome. To enable the motor to emulate a DC motor, the control system requires information about the instantaneous rotor flux position or the rotor position of a permanent magnet motor. This necessitates the use of a resolver or an absolute optical encoder. Once the position is known, the calculation of the three-phase currents can be performed. The method of calculation, utilizing the current matrix, is contingent upon the desired control objectives. Some available control options include maintaining constant torque and flux weakening, which are determined by the physical constraints of the motor and the inverter. The boundary is determined by the motor's rated speed, beyond which the constant torque operation concludes and the flux weakening phase commences, as depicted in Figure 7.

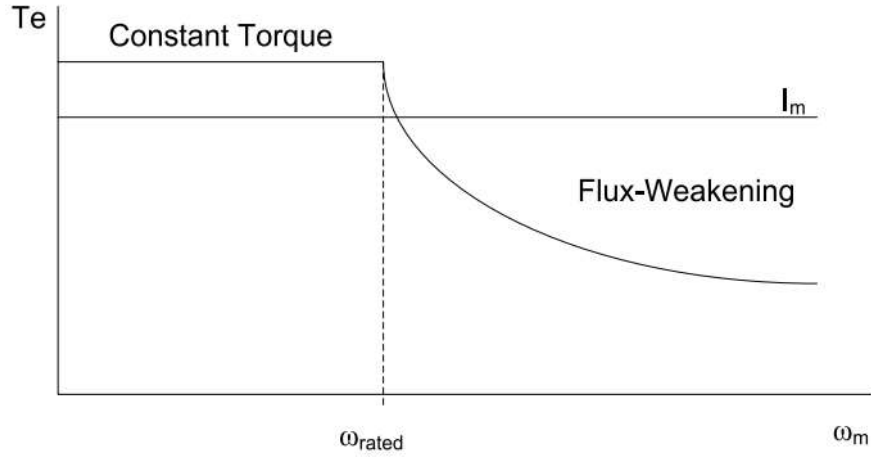


Figure 7. Constant Torque and Flux-Weakening Treatment [42]

3.3.13 Field Oriented Control of PM Motors:

The control of Permanent Magnet Synchronous Motors (PMSM) mirrors that of DC motors through a decoupling method referred to as field-oriented control or vector control. This technique disentangles the torque and flux components of current within the motor by modulating its stator excitation. The vector control strategy for PM synchronous motors is derived from their dynamic model. With the currents serving as inputs, the system evaluates the three currents:

$$i_a = I_m \sin(\omega_r t + \alpha) \quad (27)$$

$$i_b = I_m \sin\left(\omega_r t + \alpha - \frac{2\pi}{3}\right) \quad (28)$$

$$i_c = I_m \sin\left(\omega_r t + \alpha + \frac{2\pi}{3}\right) \quad (29)$$

In the matrix shape, it is defined as:

$$\begin{pmatrix} i_a \\ i_b \\ i_c \end{pmatrix} = \begin{pmatrix} \cos(\omega_r t + \alpha) \\ \cos\left(\omega_r t + \alpha - \frac{2\pi}{3}\right) \\ \cos\left(\omega_r t + \alpha + \frac{2\pi}{3}\right) \end{pmatrix} (I_m) \quad (30)$$

Where α is the angle between the rotor field and stator current phasor, ω_r is the electrical rotor speed. The stator currents previously determined need to be converted to the rotor reference frame with the rotor speed ω_r using Park's transformation. In the rotor reference frames, the q and d axis currents remain constant since α is consistent for a given load torque. Analogous to the armature and field currents in a separately excited DC machine, these constants play similar roles. The q axis current corresponds directly to the armature current of the DC machine, while the d axis current represents the field current, albeit only partially. A portion of the field current is contributed by the equivalent current source representing the permanent magnet field. Consequently, the q axis current is referred to as the torque-producing component of the stator current, while the d axis current is termed the flux-producing component of the stator current. Substituting equation 30 and 25 is obtain i_a and i_q in terms of I_m as follows

$$\begin{pmatrix} i_q \\ i_d \end{pmatrix} = I_m \begin{pmatrix} \sin \alpha \\ \cos \alpha \end{pmatrix} \quad (31)$$

Using equations 4,15,21 and 31 the electromagnetic torque equation is obtained as given below.

$$T_e = \frac{3}{2} \cdot \frac{P}{2} \left[\frac{1}{2} (L_d - L_q) I_m^2 \sin 2\alpha + \lambda_f I_m \sin \alpha \right] \quad (32)$$

3.3.14 Constant Torque Operation:

The constant torque control approach is derived from field-oriented control, aiming to maintain the maximum achievable torque consistently, similar to a DC motor. This is achieved by setting the torque-producing current i_q equal to the supply current I_m . Consequently, the α angle is chosen to be 90 degrees, as per equation 31. Setting the id current to zero allows for the torque equation to be reformulated as:

$$T_e = \left(\frac{3}{2}\right) \left(\frac{P}{2}\right) \lambda_f i_q \quad (33)$$

Assuming that:

$$k_t = \left(\frac{3}{2}\right) \left(\frac{P}{2}\right) \lambda_f \quad (34)$$

Therefore, torque is given by:

$$T_e = k_t \cdot i_q \quad (35)$$

Like the dc motor, the torque is dependent of the motor current.

3.3.15 THE FLUX-WEAKENING:

Flux weakening involves diminishing the flux in the d-axis direction of the motor, thereby extending the operational speed range. Initially, the motor drive operates with rated flux linkages until a speed is reached where the ratio between induced emf and stator frequency (V/f) remains constant. Beyond this base frequency, the V/f ratio decreases due to the fixed limit of the inverter DC voltage source. To operate above the base frequency, weakening the field flux becomes necessary, consequently reducing the V/f ratio. This operation results in a proportional reduction in torque with changes in frequency, placing the motor in the constant power region.

In Permanent Magnet Synchronous Motors (PMSM), the rotor flux, generated by permanent magnets, cannot be directly diminished as in an induction motor. Hence, the principle of flux-weakening control in PMSM involves increasing negative direct axis current and utilizing armature reaction to decrease air gap flux, thereby effectively reducing flux and achieving flux-weakening control.

This method of control alters torque by adjusting the angle between the stator MMF and the rotor d-axis. In the flux weakening region where $\omega_r > \omega_{rated}$, the angle α is managed through proper control of i_d and i_q for the same stator current magnitude. As i_q decreases, the output torque also decreases. The angle α can be determined as follows:

$$\alpha = \text{Tan}^{-1} \left(\frac{i_q}{i_d} \right) \quad (36)$$

The current I_m is related to i_d and i_q by

$$I_m = \sqrt{i_d^2 + i_q^2} \quad (37)$$

3.3.16 Speed Control of PM Motor:

Numerous applications, including robotics and factory automation, necessitate precise control over speed and position. Speed Control Systems facilitate the easy setting and adjustment of motor speed. This system typically comprises a speed feedback mechanism, a motor, an inverter, a controller, and a speed setting device. A well-designed feedback controller renders the system robust against disturbances and parameter variations.

The primary objective of a motor speed controller is to receive a signal representing the desired speed and regulate the motor to operate at that speed. Closed-loop speed control systems offer rapid response times but tend to be more costly due to the inclusion of feedback components such as speed sensors.

3.3.16.1 Implementation of the Speed Control Loop

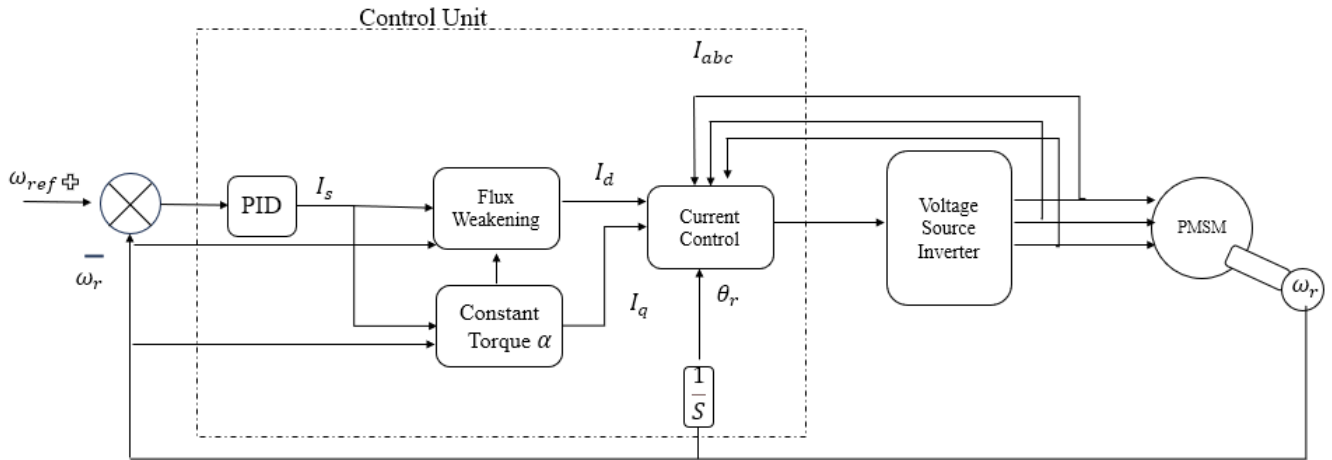


Figure 8. PMSM Motor Design

In a PM motor drive system encompassing the entire speed spectrum, the setup typically includes a motor, an inverter, and a controller. This controller, depicted in figure 8., encompasses functions such as constant torque and flux weakening operations, generation of reference currents, and PID control. The controller's operation must align with the speed range requirements. Below the rated speed, it functions within the constant torque region, while beyond the rated speed, it operates in the flux-weakening region. In this latter region, both the d-axis flux and the resulting torque are diminished. The speed controller computes the variance between the reference speed and the current speed, generating an error signal that is forwarded to the PID controller. PID controllers are extensively employed in motion control systems. They comprise a proportional gain component that yields an output proportionate to the input error, along with an integrator aimed at nullifying steady-state errors resulting from step changes in the input. The block diagram of the PID controller is illustrated in figure 9.

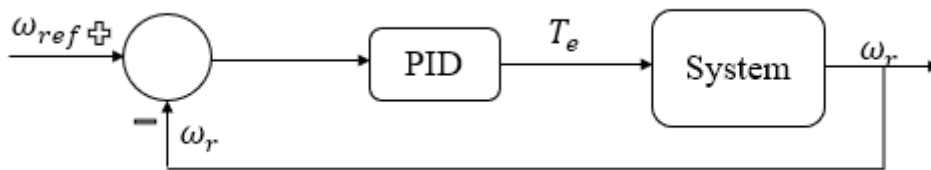


Figure 9. Illustration of PID Controller

Motor speed control typically involves two loops: an inner loop for current and an outer loop for speed. The sequencing of these loops is dictated by their respective response times, prioritizing rapid adjustment capability. Consequently, the current loop must operate at least ten times faster than the speed loop.

Given that Permanent Magnet Synchronous Motors (PMSM) are managed using field-oriented control, they can be likened to DC motors in terms of modeling. Design initiation involves the innermost current loop, typically outlined through block diagrams. However, in PMSM drive systems, the motor incorporates current controllers, thereby handling the current loop autonomously. Current control is executed through

comparing reference currents with actual motor currents. When designing the speed loop, it is assumed that the current loop operates at least ten times faster than the speed loop, simplifying the system's block diagram by considering the current loop to have unity gain.

3.4 System Control:

3.4.1 Control law for quadrotor:

The approach pursued in this thesis for system control involved assessing the PID controller technique, refining it through simulation, and then implementing the most effective and refined controller on the quadrotor. The primary focus was on attitude control, as it represents the core of the control challenge.

3.4.2 Modelling for Control:

In control design, it's recommended to simplify the model to meet the real-time demands of the embedded control loop. This involves assuming constant thrust and drag coefficients. The system can then be expressed in state-space form as $\dot{X} = f(X, U)$, where U is the input vector and X is the chosen state vector:

$$X = [\varphi \theta \psi z] \quad (38)$$

Where:

$$\begin{aligned} x_1 &= \varphi \\ x_2 &= \theta \\ x_3 &= \psi \\ x_4 &= z \end{aligned} \quad (39)$$

And

$$U = [U_1 U_2 U_3 U_4]^T \quad (40)$$

And inputs are defined as:

$$\begin{cases} U_1 = b(\Omega_1^2 + \Omega_2^2 + \Omega_3^2 + \Omega_4^2) \\ U_2 = b(-\Omega_2^2 + \Omega_4^2) \\ U_3 = b(\Omega_1^2 - \Omega_3^2) \\ U_4 = d(-\Omega_1^2 + \Omega_2^2 - \Omega_3^2 + \Omega_4^2) \end{cases} \quad (41)$$

After simplification, the following expression is obtained:

$$f(X,U) = \begin{pmatrix} \dot{\theta}\dot{\psi}a_1 + \dot{\theta}a_2\Omega_r + b_1U_2 \\ \dot{\phi}\dot{\psi}a_3 - \dot{\phi}a_4\Omega_r + b_2U_3 \\ \dot{\theta}\dot{\phi}a_5 + b_3U_4 \\ g - (\cos\varphi\cos\theta)\frac{1}{m}U_1 \end{pmatrix} \quad (42)$$

Where:

$$\begin{aligned} a_1 &= \frac{I_{yy} - I_{zz}}{I_{xx}} \\ a_2 &= \frac{J_r}{I_{xx}} \\ a_3 &= \frac{I_{zz} - I_{xx}}{I_{yy}} \end{aligned} \quad (43)$$

$$\begin{aligned} a_4 &= \frac{J_r}{I_{yy}} \\ a_5 &= \frac{I_{xx} - I_{yy}}{I_{zz}} \\ b_1 &= \frac{l}{I_{xx}} \\ b_2 &= \frac{l}{I_{yy}} \\ b_3 &= \frac{l}{I_{zz}} \end{aligned} \quad (44)$$

3.4.3 Control model of Quadrotor:

The dynamic model provided includes one gyroscopic effect, although in our scenario, their impact is less significant compared to the motor's influence, particularly when considering a near-hover situation. To facilitate the design of multiple PID controllers for this system, one can disregard these gyroscopic effects, effectively eliminating cross-coupling. Subsequently, the model is revised as follows:

$$\begin{cases} I_{xx}\ddot{\phi} = lU_2 \\ I_{yy}\ddot{\theta} = lU_3 \\ I_{zz}\ddot{\psi} = U_4 \end{cases} \quad (45)$$

If we incorporate rotor dynamics into equation 7 and transform the model into the Laplace domain, we obtain:

$$\left\{ \begin{array}{l} \varphi(s) = \frac{B^2 bl}{s^2(s+A)^2 I_{xx}} (u_4^2(s) - u_2^2(s)) \\ \theta(s) = \frac{B^2 bl}{s^2(s+A)^2 I_{yy}} (u_3^2(s) - u_1^2(s)) \\ \psi(s) = \frac{B^2 d}{s^2(s+A)^2 I_{zz}} (-1)^{i+1} \sum_{i=1}^4 u_i^2(s) \end{array} \right. \quad (46)$$

$$A = \left(\frac{1}{\tau} + \frac{2d\omega_0}{\eta r^3 J_t} \right)$$

$$B = \left(\frac{1}{km\tau} \right)$$

$$C = \left(\frac{d\omega_0^2}{\eta r^3 J_t} \right)$$

In this context, A and B represent the coefficients of the linearized rotor dynamics, while C, being considerably smaller than B, is disregarded. Transitioning from motor inputs u_i to control inputs U_i , the preceding equation transforms into:

$$\left\{ \begin{array}{l} Z(s) = g - \frac{1}{m} U_1 \\ \varphi(s) = \frac{A^2 l}{s^2(s+A)^2 I_{xx}} U_2 \\ \theta(s) = \frac{A^2 l}{s^2(s+A)^2 I_{yy}} U_3 \\ \psi(s) = \frac{A^2}{s^2(s+A)^2 I_{zz}} U_4 \end{array} \right. \quad (47)$$

3.4.4 PID Controller Design for quadrotor:

By using simulation parameters and referencing measurements for inputs, the error can be obtained through comparison or analysis.

$$\begin{aligned} Z^{optimized} &= Z^{ref} - Z^{sim} \\ \varphi^{optimized} &= \varphi^{ref} - \varphi^{sim} \\ \theta^{optimized} &= \theta^{ref} - \theta^{sim} \\ \psi^{optimized} &= \psi^{ref} - \psi^{sim} \end{aligned} \quad (48)$$

3.4.5 Control model for PMSM:

To control the rotational speed of a Permanent Magnet Synchronous Motor (PMSM) using a PID controller, a series of steps must be followed. This process includes modeling the motor, designing the PID controller, and implementing it. Below are the equations and the detailed steps that will be explained:

3.4.6 PMSM Motor Model:

The dynamics of a PMSM can be represented in the dq-frame (rotating reference frame) using the following equations:

$$\begin{aligned} v_d &= R_s i_d + L_d \frac{di_d}{dt} - \omega_r L_q i_q \\ v_q &= R_s i_q + L_q \frac{di_q}{dt} + \omega_r L_d i_d + \lambda_f \omega_r \end{aligned} \quad (49)$$

Where:

v_d, v_q	Are the dq-axis voltages
i_d, i_q	Are the dq-axis currents
R_s	Is the stator resistance
L_d, L_q	Are the dq-axis inductances
ω_r	Is the rotor angular velocity (electrical rad/s)
λ_f	Is the flux linkage due to the permanent magnet

3.4.6.1 Mechanical Equation:

$$J \frac{d\omega_r}{dt} = T_e - T_L - B\omega_r \quad (50)$$

Where:

J	Is the rotor inertia
T_e	Is the electromagnetic torque
T_L	Is the load torque
B	Is the viscous friction coefficient

The electromagnetic torque T_e can be given by:

$$T_e = \frac{3}{2} P \left(\lambda_f i_q + (L_d - L_q) i_d i_q \right) \quad (51)$$

For surface-mounted PMSMs, $L_d = L_q$, simplifying the torque equation to:

$$T_e = \frac{3}{2} P \lambda_f i_q \quad (52)$$

3.4.6.2 Speed Control Loop:

The objective is to control the motor speed ω_r . The PID controller will be designed for the speed loop.

3.4.6.3 PID Controller Design:

The PID controller for speed control is designed to generate a reference torque T_e^{ref}

3.4.6.4 Speed Error:

$$e_\omega(t) = \omega_r^{ref}(t) - \omega_r(t) \quad (53)$$

3.4.6.5 PID Controller:

$$T_e^{ref}(t) = K_p e_\omega(t) + K_i \int e_\omega(t) dt + K_d \frac{de_\omega(t)}{dt} \quad (54)$$

Where:

K_p Is the proportional gain

K_i Is the integral gain

K_d Is the derivative loop

3.4.6.6 Current Control Loop:

The reference torque T_e^{ref} is used to generate the i_q^{ref} current, assuming $i_d = 0$ (for maximum torque per ampere control).

$$i_q^{ref} = \frac{2T_e^{ref}}{3P\lambda_f} \quad (55)$$

And

$$i_q^{optimized} = i_q^{ref} - i_q^{sim} \quad (56)$$

3.4.6.7 Current Controller (PID Controller):

A PID controller is typically used for the current loop to track i_q^{ref} .

d-axis current controller:

$$v_d^{ref} = K_{pd}(i_d^{ref} - i_d) + K_{id} \int (i_d^{ref} - i_d) dt + K_{dd} \frac{d(i_d^{ref} - i_d)}{dt} \quad (57)$$

And q-axis current controller:

$$v_q^{ref} = K_{pq}(i_q^{ref} - i_q) + K_{iq} \int (i_q^{ref} - i_q) dt + K_{dq} \frac{d(i_q^{ref} - i_q)}{dt} \quad (58)$$

Where:

K_{pd}, K_{id}, K_{dd} . are the proportional, integral and derivative gains for the d-axis current controller

K_{pq}, K_{iq}, K_{dq} . are the proportional, integral and derivative gains for the q-axis current controller

However, this aspect was neglected in the thesis because of the faster current dynamics.

3.5 OPTIMIZATION METHOD

3.5.1 The conceptual framework:

Kennedy and Eberhart introduced PSO in 1995 based on the premise that members of a fish school can benefit from the collective discoveries and experiences of others, as proposed by sociobiologist Edward O. Wilson in 1975. PSO operates on the principle that candidate solutions in an optimization problem form a swarm of particles moving through parameter space, guided by their own and neighboring particles' best performances. In essence, PSO allows particles to learn from each other's past experiences. This contrasts with traditional nature-inspired methods such as genetic algorithms, where improvements are typically made through different mechanisms. In PSO, cooperation and competition among individuals drive the process of improvement.

3.5.2 The fundamental PSO method:

As previously said, a swarm is a group of simple, well-organized individuals operating independently of a leader. Let's substitute "particle" for "individual." The position x of particle i , defined as x_i , is one possible solution to the optimization issue. Thus, the following could be a possible solution if we're trying to optimize D parameters:

$$x_i = (x_{i1}, x_{i2}, \dots, x_{iD}), \quad (59)$$

and N particles x constitutes a swarm, defined as X :

$$X = (x_1, x_2, \dots, x_N), \quad (60)$$

Consider a scenario where a flock of birds (X) is in search of food. Each bird within the flock directs its attention to a particular direction determined by its current position. Subsequently, they engage in communication, enabling identification of the bird occupying the optimal position. Once the "best bird" is established, each bird adjusts its movement velocity based on its current velocity and additional insights gleaned from the collective. This iterative process continues until the desired position is reached. To express this behavior mathematically, we need to revisit 1995, when the initial proponents of PSO introduced their model. They suggested that each particle's position evolves according to a specific equation:

$$x_i^{t+1} = x_i^t + v_i^{t+1}, \quad (61)$$

where v_i^{t+1} is the updated velocity defined as:

$$v_i^{t+1} = \omega_{ps0} v_i^t + 2R_1(p_i - x_i^t) + 2R_2(g - x_i^t) \quad (62)$$

Thus, the velocity, a D -dimensional vector, signifies that each coordinate possesses a distinct velocity. As particles are continuously in motion, we denote "t" as a fixed moment. Hence, the position x_i^t represents the particle's location at that specific time instance "t". Subsequently, the particle will transition with velocity v_i^{t+1} to attain position x_i^{t+1} . This sequence, encompassing all N particles, constitutes an iteration and ω_{ps0} is inertia weight. Three factors aid in defining velocity at $t + 1$:

- v'_i which corresponds to velocity at t is also called *inertia* or *momentum* and prevents the particle from drastically changing its direction.
- $2R1(pi - xit)$, where $R1$ is a randomly generated number from a uniform distribution in the $[0,1]$ interval and pi is the best position attained by particle i . This part is called cognitive component and corresponds to the individual intelligence of the particle. This term increases the probability that the particle returns to their previously best position found,
- $2R2(g - xit)$, where g is the global best, that is, the best position attained by the whole swarm of particles at moment t , and $R2$ is a randomly generated number similar to $R1$. The whole term is called *social component* and identifies the propensity of a particle to move towards the best position

Two further observations are necessary for a comprehensive understanding of equation 60. Firstly, the presence of $R1$ and $R2$ serves to introduce stochastic elements, ensuring that both the social and cognitive components influence the overall velocity change unpredictably. Secondly, a contrasting perspective elucidates why the constants $c1$ and $c2$ are set to a value of 2.

As per Kennedy and Eberhart's 1995 paper, setting $c1 = c2 = 2$ ensures that the weights for the social and cognitive components average to 1, facilitated by the random uniform aspect. Despite attempting various enhancements to this PSO version, their most notable effort involved introducing two additional roles: the "explorer" and the "settler". While explorers were tasked with seeking distant potential locations from the target, settlers were responsible for exploring promising regions in finer detail. Ultimately, the simpler version appeared to yield superior results.

3.5.3 Algorithm:

We've observed various strategies for optimizing the same method, but in this section, we'll focus solely on the basic PSO algorithm. We believe that the steps outlined here can be adapted to any of the modifications we've discussed. In essence, excluding the initialization phase, the algorithm operates as follows when aiming to minimize:

```

for each iteration  $t$  do
  for each particle  $i$  do
    calculate  $v^{t+1}$ 
    update  $x^{t+1}$ 
    calculate  $f(x^{t+1})$ 
    if  $f(x^{t+1}) < f(p)$  then
      | update  $p$ 
    end
    if  $f(x^{t+1}) < f(g)$  then
      | update  $g$ 
    end
  end
end
end

```

3.5.4 FLOWCHART of PSO:

The flowchart of PSO algorithm is shown as figure 10:

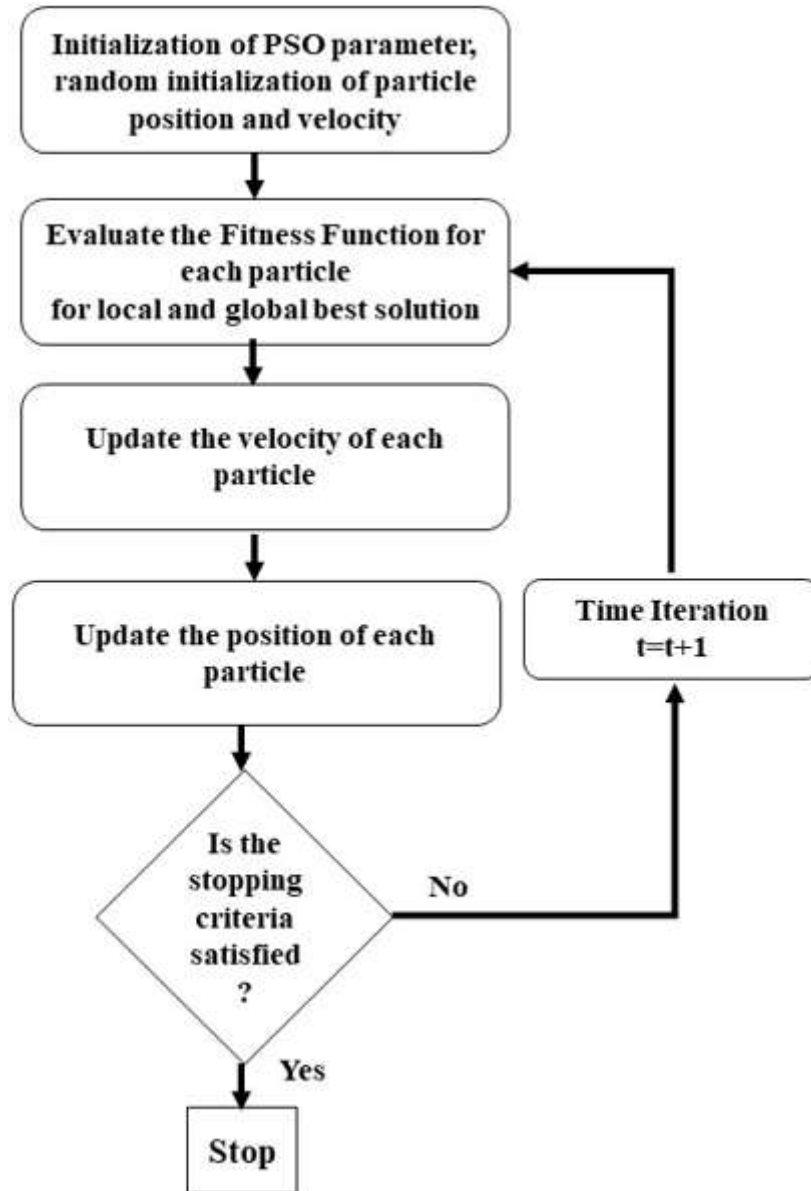


Figure 10. Flow Chart of PSO [43]

4. Chapter 4

4.1 Simulation Setting:

4.1.1: Quadrotor Simulation Setting:

The simulation was done in Simulink within the MATLAB software, as shown in Figure 11. This part was composed of three blocks:

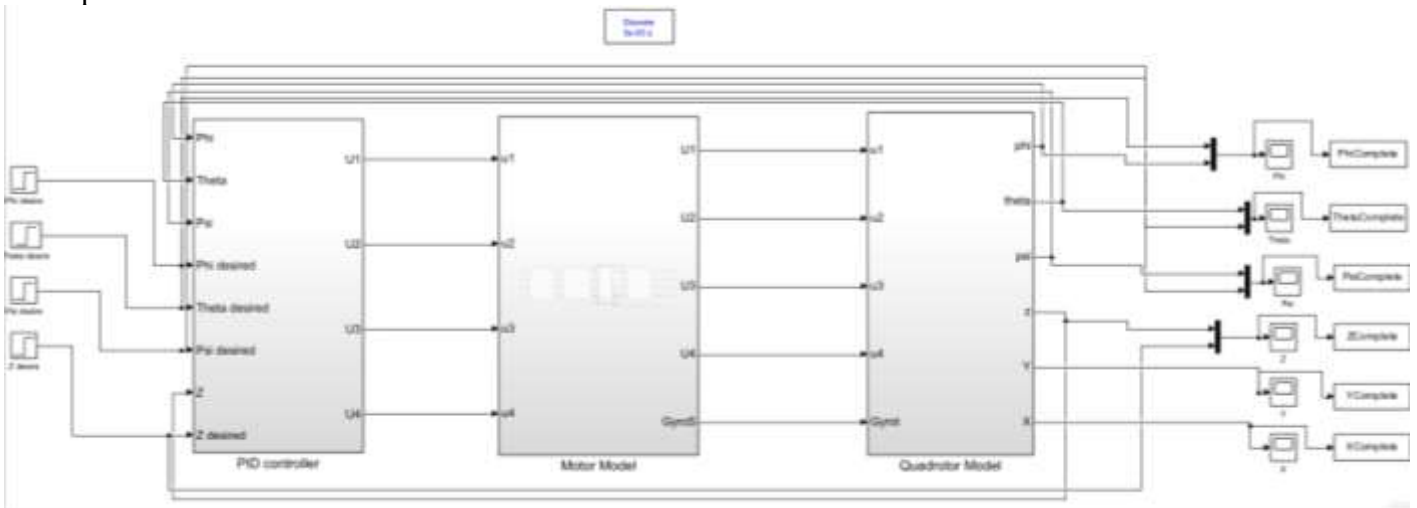


Figure 11. Complete model

4.1.1.1: PID controller block:

In this section, as shown in Figure 12, the PID controller was designed with respect to the inputs:

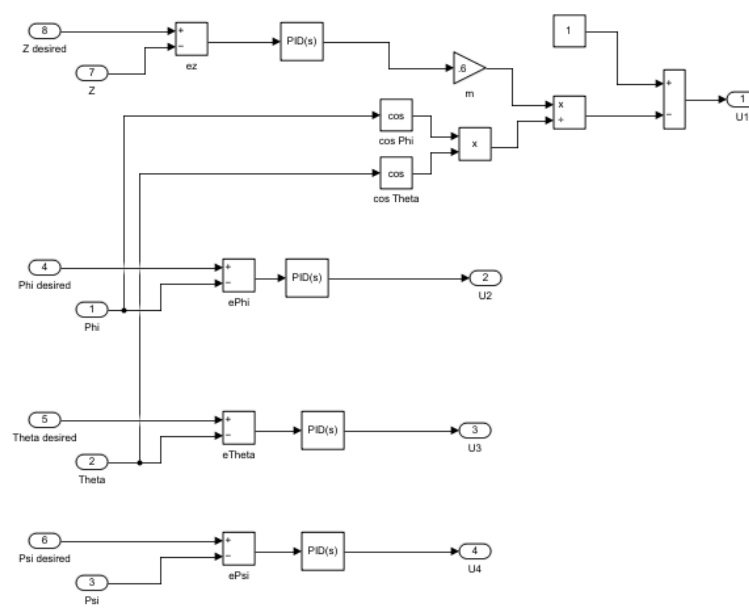


Figure 12: PID Controller model

4.1.1.2: Motor model block:

This block, as demonstrated in Figure 13, contains Equation 11, three-phase Permanent Magnet Synchronous Motors (PMSM), and gyros:

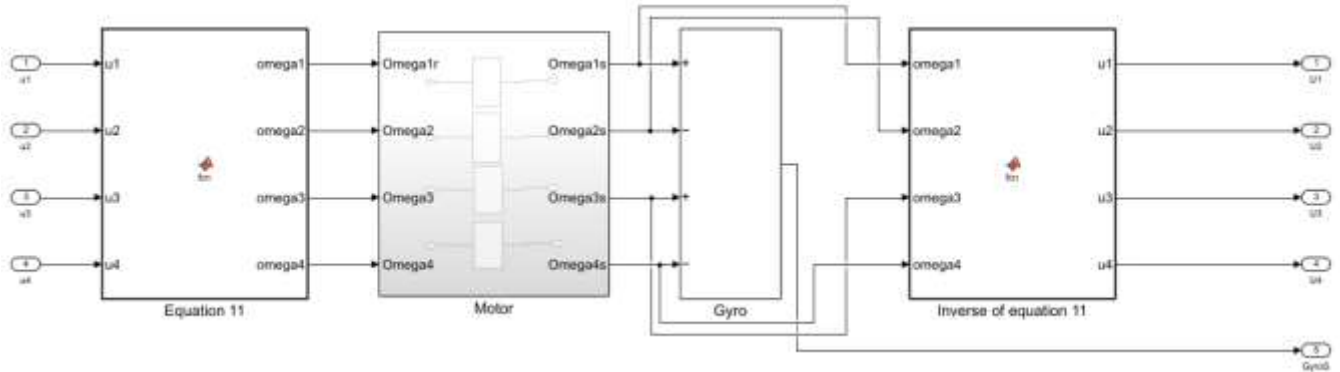


Figure 13. Motor model

The PMSM motor block is demonstrated in Figure 14:

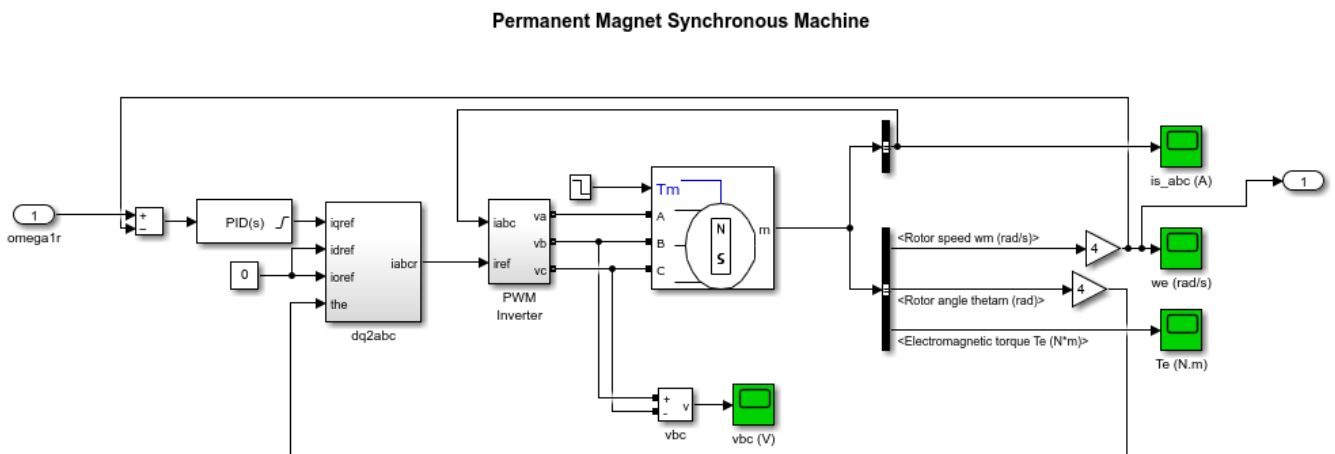


Figure 14: The Permanent Magnet Synchronous Machine Model

4.1.1.3: Quadrotor Model Block:

This block, as demonstrated in Figure 15, includes rotational dynamics, body-to-fixed frame transformation, and translation dynamics in the fixed frame:

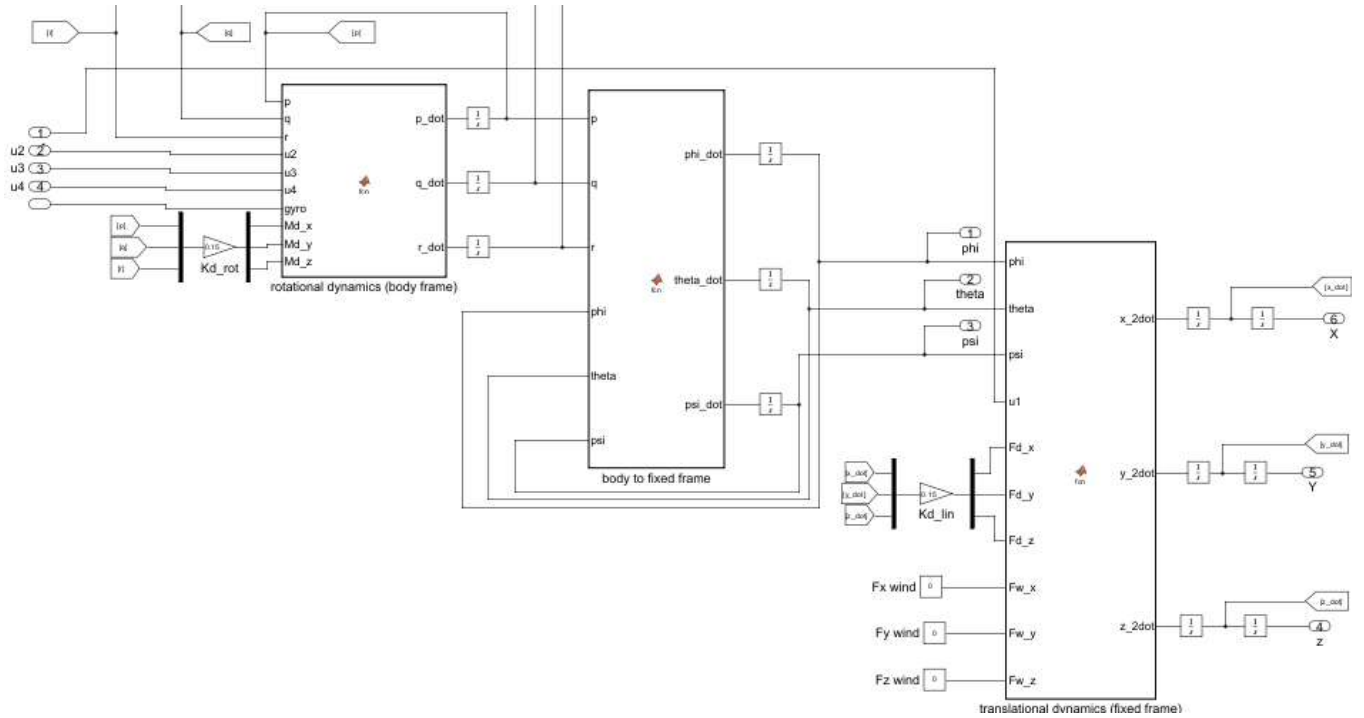


Figure 15. Complete model of quadrotor

4.2 Simulation Results:

This section covers the simulation of two typical quadrotor actions—hovering and maneuvering—conducted in MATLAB's Simulink. The PSO algorithm was employed to optimize specific parameters to enhance the quadrotor's stability and controllability. The results from simulations with both optimized and non-optimized parameters are discussed in this section. In the simulation section, the sequence of instructions will be followed. In the first part, the PID parameters for the quadrotor, excluding the motors, will be obtained. In the second part, the rotational speed according to equation (11) will be determined, and each motor will be simulated and controlled by PID, then optimized using the PSO algorithm. In the third step, the complete quadrotor simulation will be demonstrated.

4.2.1 Simulation Parameter:

The initial parameters for the quadrotor and motors, necessary for simulations of both hovering and maneuvering actions, are listed in Tables 1.

Simulation Parameter Type	Parameter	Value
UAV	m	0.6kg
	g	9.81
	b	$3.6 \times 10^{-6} \text{ kg.m}$
	d	$1.6 \times 10^{-7} \text{ kg.m}^2$
	I_x	$5.2 \times 10^{-3} \text{ kg.m}^2$
	I_y	$5.2 \times 10^{-3} \text{ kg.m}^2$
	I_z	$9.4 \times 10^{-3} \text{ kg.m}^2$
	I_R	$4.5 \times 10^{-5} \text{ kg.m}^2$
	L	0.02m

	K_d^R	$0.15kg.m^2.s^{-1}$
	K_d^L	$0.15kg.s^{-1}$
PMSM	Number of Phases	3
	Back EMF waveform	Sinusoidal
	Rotor type	Round
	Mechanical input	Torque
	Preset model	NO

4.2.2 Hovering:

The concept of a quadrotor's hovering model refers to its capability to stay in a stable position in the air without any horizontal or vertical movement. This crucial function necessitates precise control over the quadrotor's motors to counterbalance the various forces and torques acting upon it. Consequently, the parameters phi, psi, theta, and z, which are unique to research, will be delineated as follows:

Table2: initial parameters for Hovering	
Phi	0.03 (rad)
Psi	0.03(rad)
Theta	0(rad)
Z	5(m)

Through the consideration of particular parameters and measurements related to PID variables, the Simulink outcomes will be obtained and presented as figure 16:

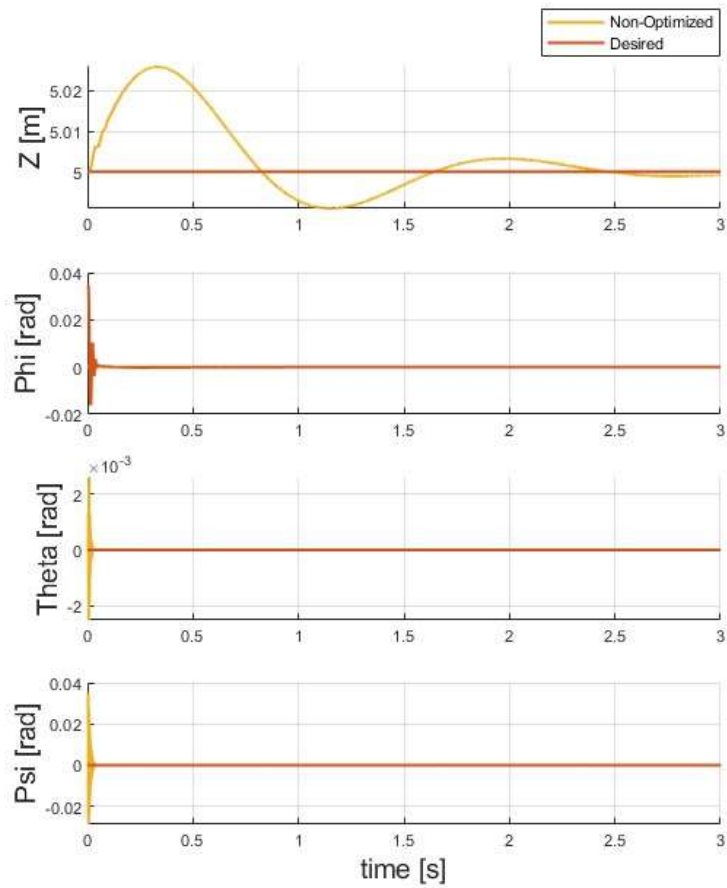


Figure 16: non-optimization results for Hovering

In the following step, PSO is employed to optimize the PID settings for each specific parameter, as shown in figure 17:

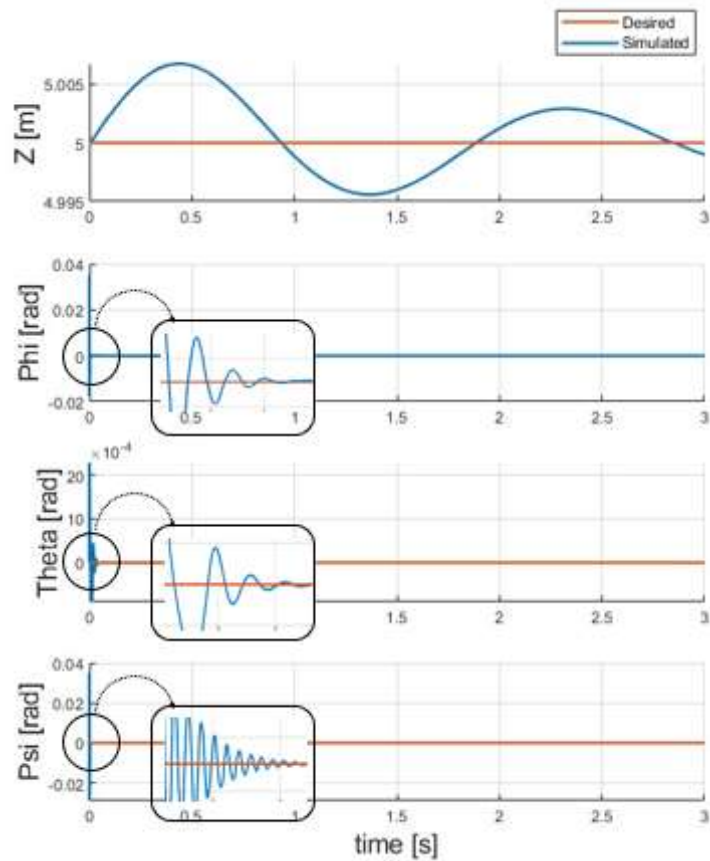


Figure 17: optimized result of Hovering

The comparison between optimized and non-optimized parameters is as follows. Figure 18 shows that both optimized and non-optimized systems take the same amount of time to stabilize. However, the optimized system experiences significantly shorter and smaller oscillations compared to the non-optimized one. This demonstrates the impact of PSO in identifying the appropriate measurements for specific parameters

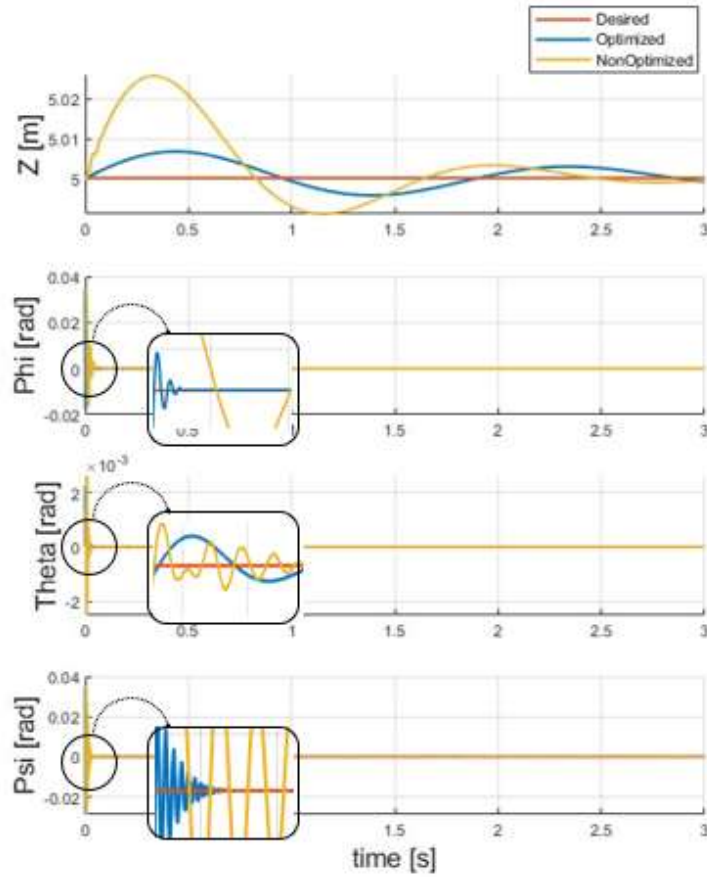


Figure 18: Comparing optimize and non-optimize control of PID in Hovering

Moreover, by considering the best cost functions of both optimized and non-optimized cases, the modification of the optimization method can be described as follows:

Optimized	Non-optimized
5.239×10^{-4}	1.4968×10^{-3}

By optimizing the quadrotor control, the rotational speed is determined and linked to the motor. This speed is then further optimized using a PID controller and PSO. The resulting rotational speed will be:

ω_1	1020 (rad/s)
ω_2	1020 (rad/s)
ω_3	1020 (rad/s)
ω_4	1020 (rad/s)

By ensuring each motor rotates at the same speed, the convergence of the rotational speed between one motor as shown in table 3, the reference speed obtained from the quadrotor, and the PMSM motor will be shown as follows:

¹ Standard Error

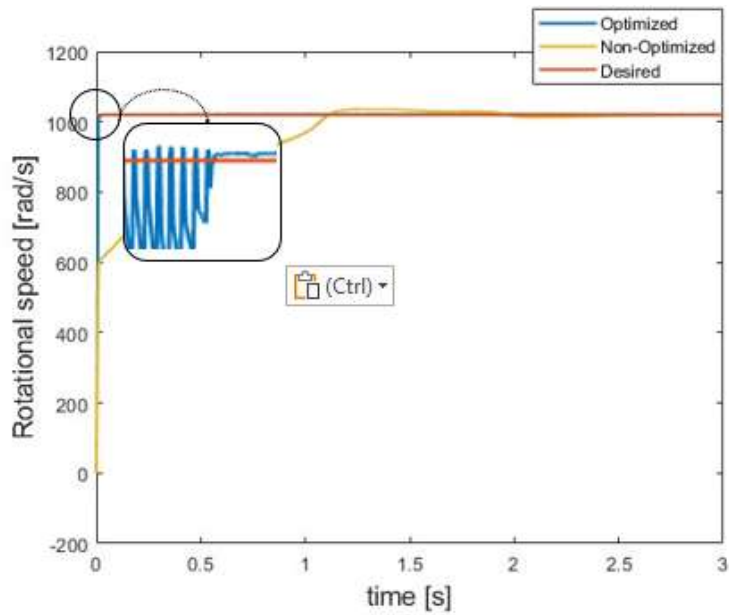


Figure19: Result of the Controlled Rotational Speed

Referring to Figure 19, optimizing the input parameters for the motors shows the effectiveness of PSO in achieving rapid stabilization of the rotational speed. In summary, optimizing the parameters for both the quadrotor and the motor will yield a complete simulation of the hovering action, shown in figure 20.

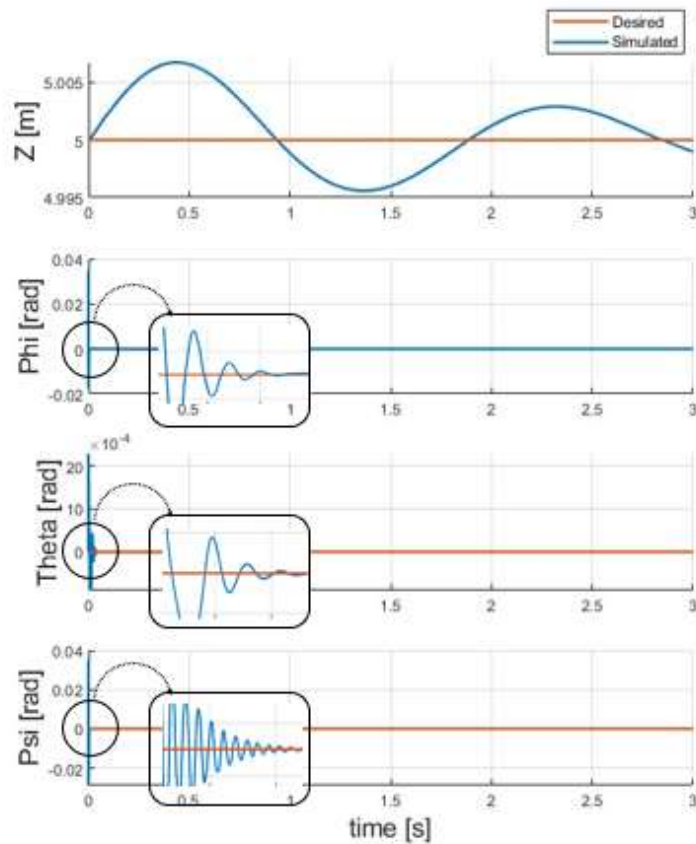


Figure 20: Complete Result of Controlled UAVs in Hovering

Considering the results obtained from the comparison, it can be inferred that optimizing the PID action for the Z parameters would suffice. This is indicated by the decreased frequency of convergence and the shorter time taken to reach the desired measurement.

The complete comparison between optimized and non-optimized UAVs during the hovering phase is done and SE obtained in the Table 4 and the result is demonstrated in figures 21 and 22:

Table 5: Comparison of (SE) for Optimized and Non-Optimized Hovering	
Optimized	Non-Optimized
1.4871×10^{-3}	3.3694×10^{-3}
5.4307×10^{-4}	1.7006×10^{-3}
1.2981×10^{-3}	5.0152×10^{-3}
7.1667×10^{-4}	1.1154×10^{-3}
2.7045×10^{-3}	7.8514×10^{-3}

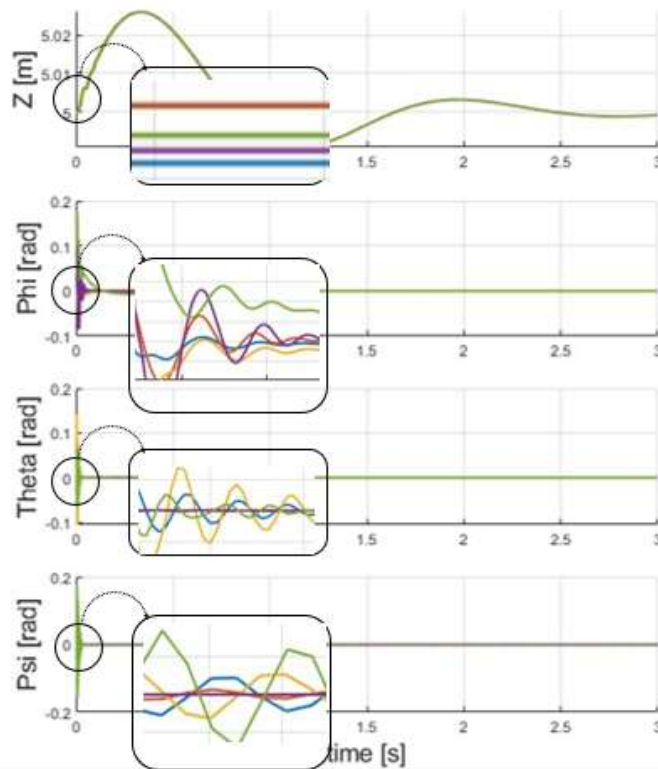


Figure 20: Non-optimized Results of Random Initial Parameters for Hovering Controller.

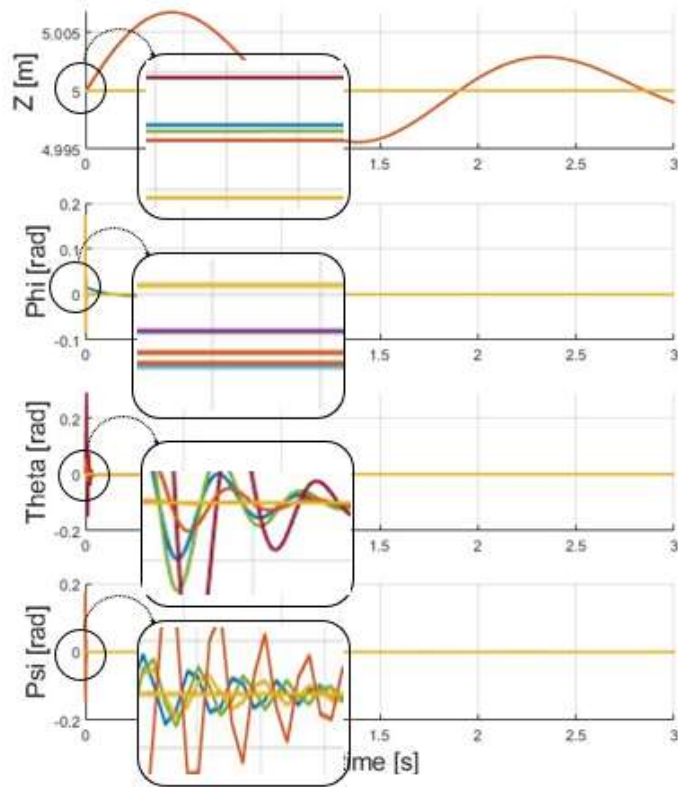


Figure 21: Optimized Results of Random Initial Parameters for Hovering Controller.

4.2.3 Maneuvering:

Maneuvering in a quadrotor" refers to the actions and techniques involved in controlling the movement and flight of a quadrotor, which is a type of drone or UAV (Unmanned Aerial Vehicle) that has four rotors. This includes tasks such as changing altitude, adjusting direction, performing turns, and executing complex flight patterns. Hence, in this section, following the outlined sequence of preceding actions, the initial step entails defining the desired parameters for specific variables as outlined defined in table5:

Table 6: Initial parameters for Maneuvering		
Parameters	Initial	Desired
Phi	0.087(rad)	0
Psi	0(rad)	0
Theta	0.087(rad)	0
Z	5(m)	10(m)

The outcomes of the non-optimized PID for the specified parameters of the quadrotor will be displayed as figure 22:

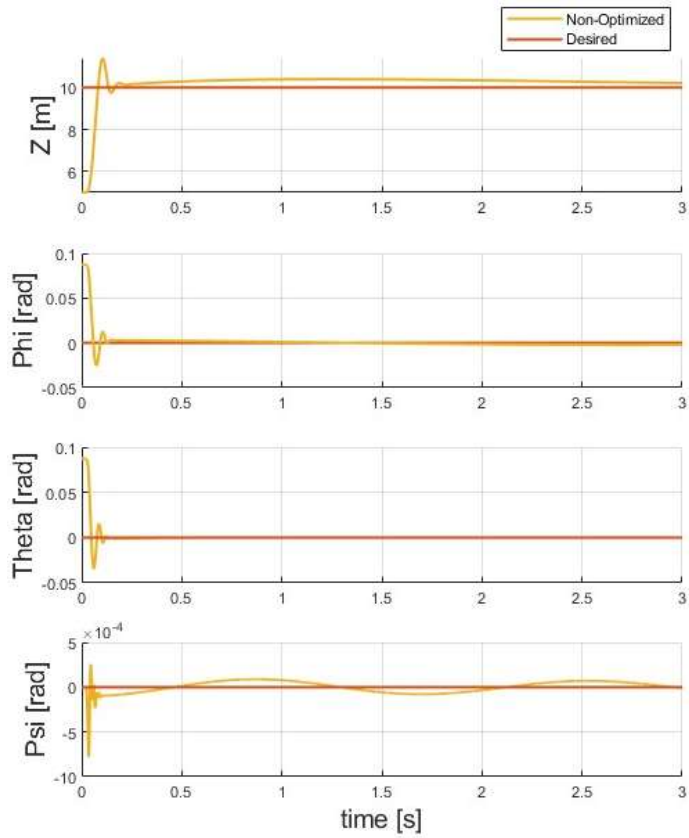


Figure 22. Non-Optimization Results for Maneuvering

Presently, with PSO taken into account, the PID parameters will be optimized, and the resultant outcome will be showcased as figure 23:

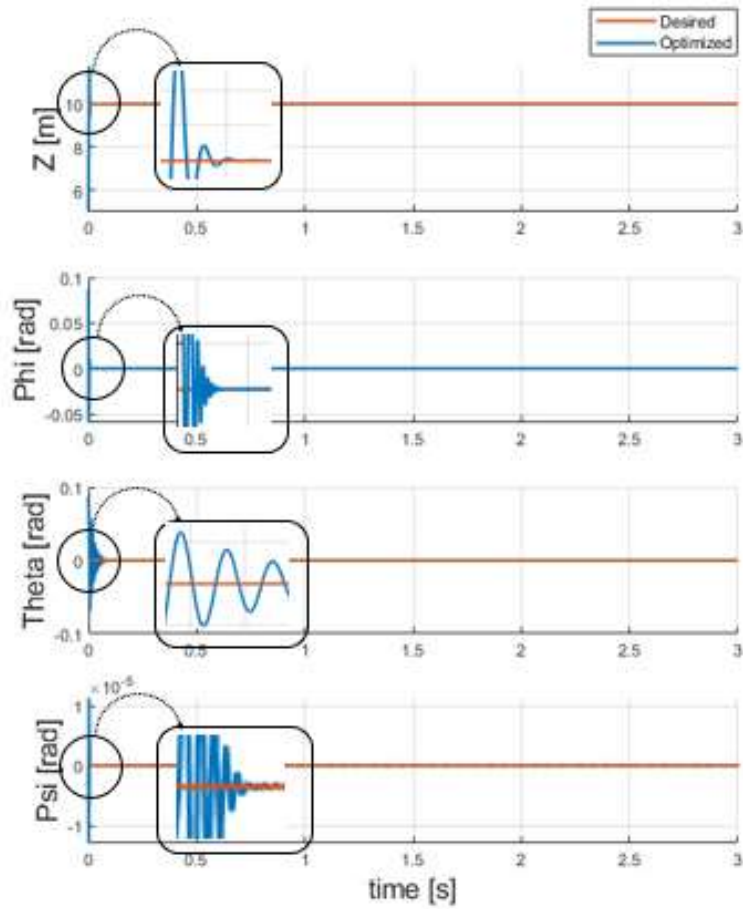


Figure 23: optimized result of Maneuvering

Table 7: Comparison of SE between Optimized and Non-Optimized Methods for Maneuvering.	
Optimized	Non-Optimized
7.3222×10^{-3}	0.0344

The comparison between the optimized and non-optimized versions will be carried out, as figure 24, The effectiveness of optimization is evident not only in significantly reducing oscillation but also in rapidly converging to the desired measurement for all parameters related to UAV altitude.

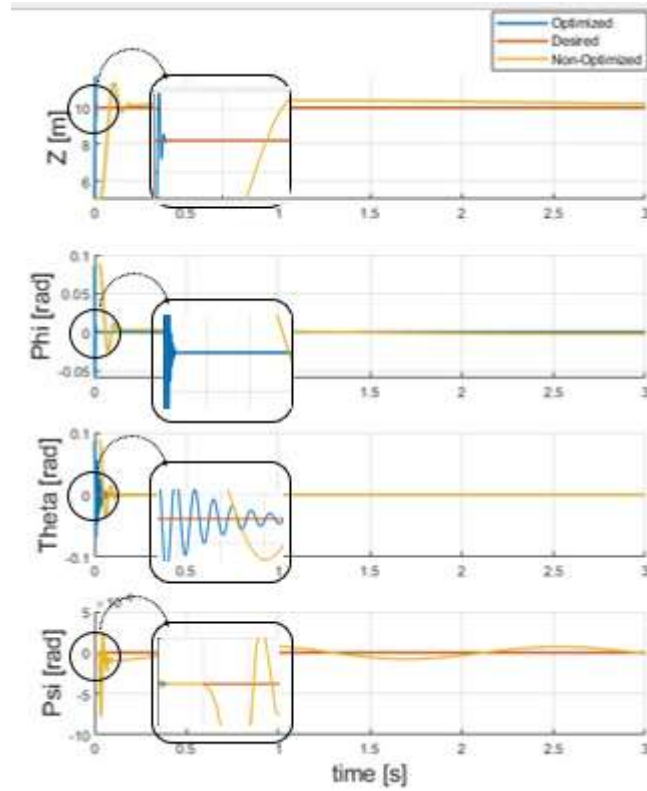


Figure 24: Comparing Optimized and Non-Optimized PID Control for Maneuvering

In this step, adhering to the optimized parameters, the rotational speed for each propeller will be determined as table 7:

Table 8: rotational speed for four motors	
ω_1	723.8 rad/s
ω_2	676.1 rad/s
ω_3	723.8 rad/s
ω_4	676.1 rad/s

By following the measurements for the propellers, it is clear that the rotational speeds of each propeller 1 and 3 are the same, as well as those of propellers 2 and 4. Consequently, after optimizing the PID for the motors as demonstrated in figure 25 and 26:

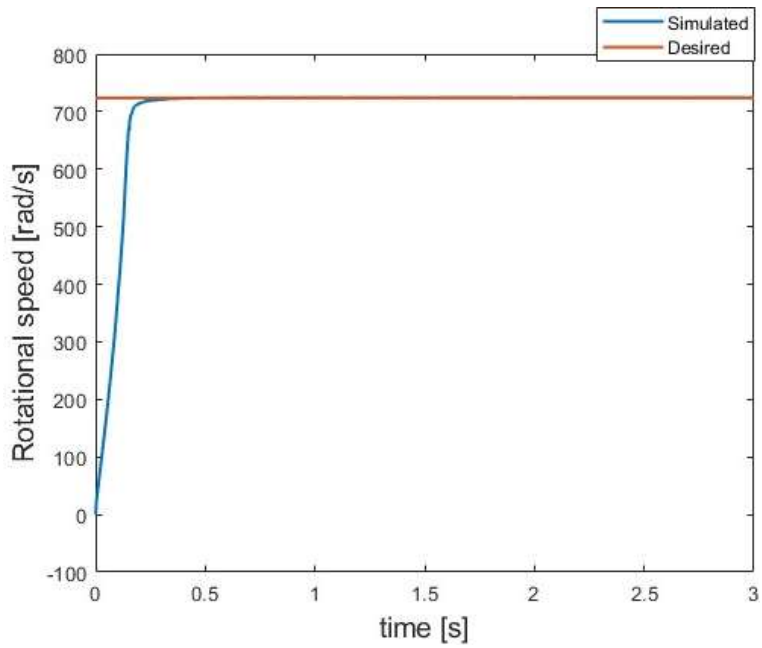


Figure25: Result of the Controlled Rotational Speed for Motors 1,3

And Motors 2 and 4 is demonstrated:

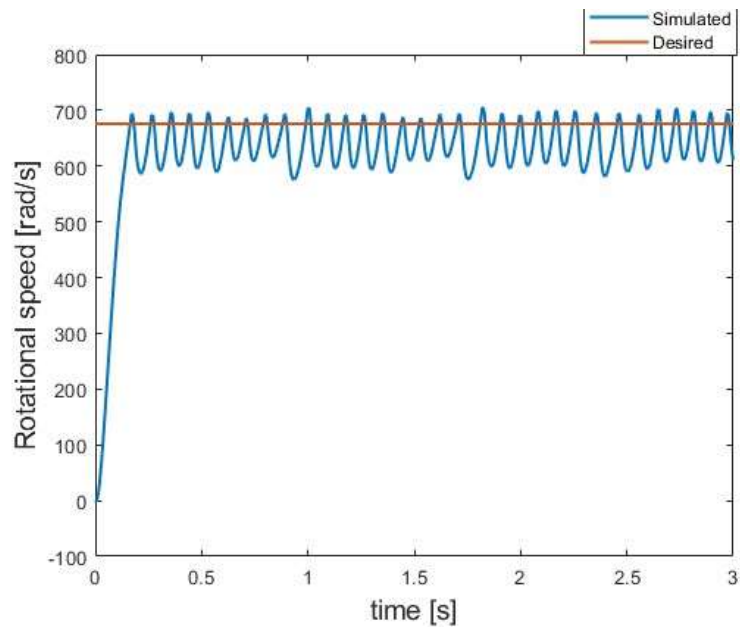


Figure 26: Result of the Controlled Rotational Speed for Motors 2,4

Now, the complete simulation results for the quadrotor in the maneuvering phase are demonstrated in the figure 27:

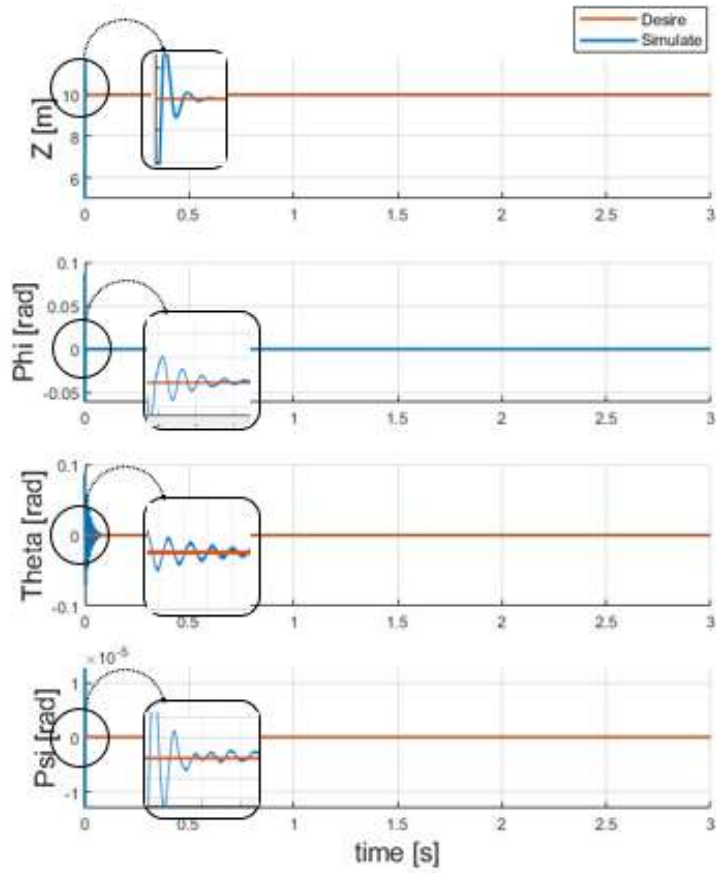


Figure 27: Complete Result of Controlled UAVs in Maneuvering

The complete comparison between optimized and non-optimized UAVs during the hovering phase is done and SE obtained in the Table 8 and the result is demonstrated in figures 28 and 29:

Optimized	Non-Optimized
0.054	0.0819
0.0286	0.0687
0.0461	0.1087
1.6752×10^{-3}	5.0549×10^{-3}
0.09856	0.1292

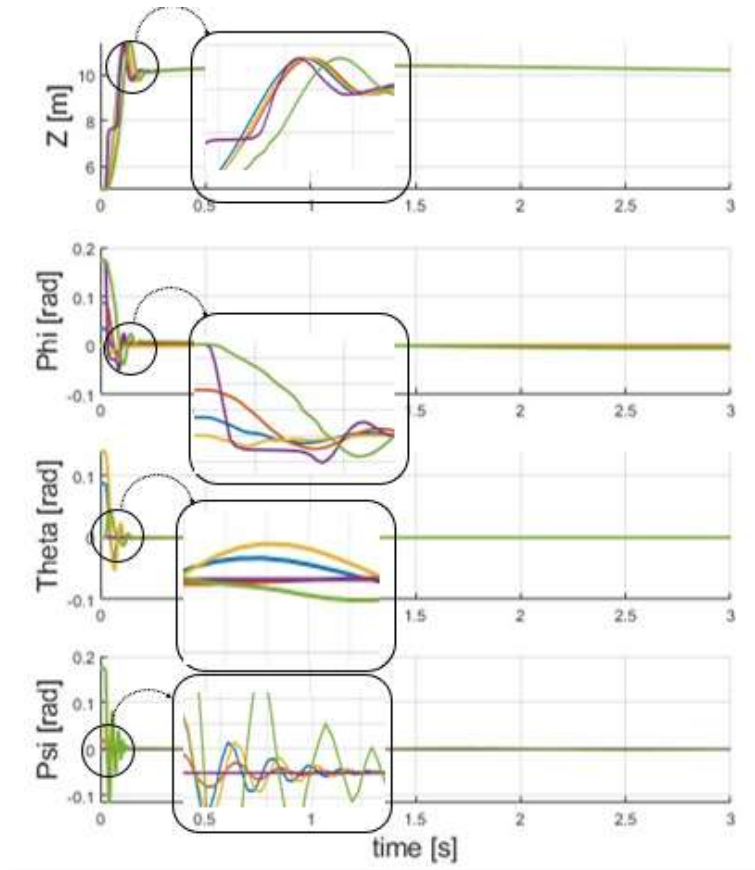


Figure 28: Non-optimized Results of Random Initial Parameters for Maneuvering Controller.

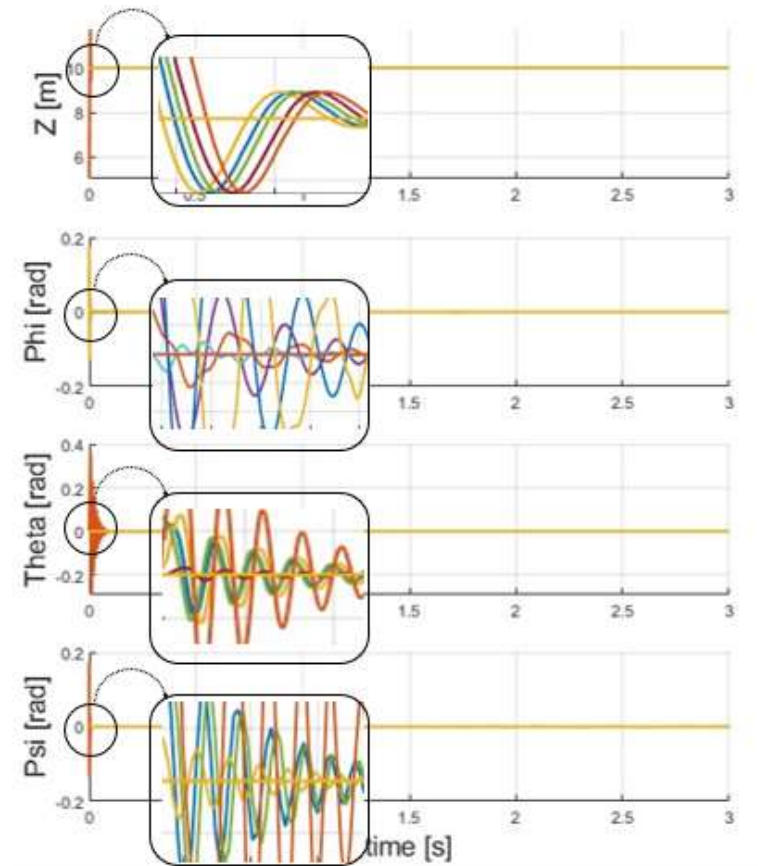


Figure 29: Optimized Results of Random Initial Parameters for Maneuvering Controller.

Reference:

- [1] Rinaldi, M.; Primatesta, S., Bugaj, M.; Rostáš, J., Guglieri, G, "Development of Heuristic Approaches for Last-Mile Delivery TSP with a Truck and Multiple Drones," *Drones*, vol. 7, 2023, doi: <https://doi.org/10.3390/drones7070407>.
- [2] M. Rinaldi, S. Primatesta, G. Guglieri, A. Rizzo, "Auction-based Task Allocation for Safe and Energy Efficient UAS Parcel Transportation," *Transportation Research Procedia*, vol. 65, pp. 60-69, 2022, doi: <https://doi.org/10.1016/j.trpro.2022.11.008>.
- [3] M. Rinaldi, S. Primatesta, G. Guglieri and A. Rizzo, "Multi-Auctioneer Market-based Task Scheduling for Persistent Drone Delivery,," presented at the 2023 International Conference on Unmanned Aircraft Systems (ICUAS), Warsaw, Poland, , 2023.
- [4] P. G. Fahlstrom, T. J. Gleason, P. Belobaba, J. Cooper, R. Langton, and A. Seabridge, *Introduction to UAV Systems*. Wiley, 2012.
- [5] J. B. Keyur Patel, "Modeling simulation and control study for the quad-copter UAV," presented at the 2014 9th International Conference on Industrial and Information Systems (ICIIS), Gwalior, India, 12 February 2015, 2015.
- [6] L. I. Weiyong Tian, Xiaohui Zhang, Dun Yang, "Double-layer fuzzy adaptive NMPC coordinated control method of energy management and trajectory tracking for hybrid electric fixed wing UAVs," *International Journal of Hydrogen Energy*,, vol. 47, no. 92, pp. 39239-39254, 2022. [Online]. Available: <https://doi.org/10.1016/j.ijhydene.2022.09.083>.
- [7] A. T. A. D. S. H. C. T. E. Fernando, M. D. C. De Zoysa, K. A. D. C. Dilshan and S. R. Munasinghe, "Modelling simulation and implementation of a quadrotor UAV," presented at the IEEE 8th International Conference on Industrial and Information Systems, Peradeniya, Sri Lanka, 2013.
- [8] S. Bouabdallah, P. Siegwart, "Design and control of an indoor micro quadrotor," presented at the In Proceedings of the IEEE International Conference in Robotics and Automation, New Orleans, LA, USA, 2004.
- [9] S. Bouabdallah, "Design and Control of Quadrotors with Application to Autonomous Flying," Ph.D. Dissertation, Ecole Polytechnique Federale de Lausann, Lausanne, Suisse, 2007.
- [10] Y. S. Naidoo, Riaan & Bright, "Quad-Rotor Unmanned Aerial Vehicle Helicopter Modelling & Control," *International Journal of Advanced Robotic Systems*, vol. 8, pp. 139–149, 2011.
- [11] I. L. A. Taame, A. Abouloifa, "Modeling of an unmanned aerial vehicle and trajectory tracking control using backstepping approach,," *IFAC-PapersOnLine*,, vol. 55, no. 12, pp. 276-281, 2022, doi: <https://doi.org/10.1016/j.ifacol.2022.07.324>.
- [12] K. B. Patel, Jayesh, "Modeling simulation and control study for the quad-copter UAV," presented at the 9th International Conference on Industrial and Information Systems, 2015.
- [13] Y. B. Kuhlmann, "A Newton Euler Approach to Modeling of a Quad-Rotor Autonomous Airship - Preliminary Results" presented at the Conference: 48th AIAA Aerospace Sciences Meeting Including the New Horizons Forum and Aerospace Exposition, 2010.
- [14] M. Rinaldi, S. Primatesta, G. Guglieri, "A Comparative Study for Control of Quadrotor UAVs," *Applied Sciences*, 2023, doi: <https://doi.org/10.3390/app13063464>.
- [15] H. P. Hanwoong Ahn, Changhyun Kim & Hyungwoo Lee, "A Review of State-of-the-art Techniques for PMSM Parameter Identification," *Journal of Electrical Engineering & Technology* vol. 15, pp. 1177–1187, 2020, doi: <https://doi.org/10.1007/s42835-020-00398-6>.

- [16] M. S. R. a. J.-W. Jun, "A Comprehensive Review of State-of-the-Art Parameter Estimation Techniques for Permanent Magnet Synchronous Motors in Wide Speed Range," *IEEE Transactions on Industrial Informatics*, vol. 16, pp. 4747-4758, 2020, doi: 10.1109/TII.2019.2944413.
- [17] N. B. R. Sadou, F. Auger and D. Pitance, "Design Optimization of an Outer Rotor PMSM for Electrical fixed-wing UAV Application Considering the Torque/RPM Working Cycle" presented at the IEEE International Electric Machines & Drives Conference (IEMDC, Hartford, CT, USA, 2021.
- [18] O. Solomon and P. Famouri, "Dynamic Performance of a Permanent Magnet Brushless DC Motor for UAV Electric Propulsion System - Part I, presented at the IECON 2006 - 32nd Annual Conference on IEEE Industrial Electronics,, Paris, France,, 2006.
- [19] X. Huo, M. Huo, and H. R. Karimi, "Attitude Stabilization Control of a Quadrotor UAV by Using Backstepping Approach," *Mathematical Problems in Engineering*, vol. 2014, p. 749803, 2014/02/19 2014, doi: 10.1155/2014/749803.
- [20] R. Roy, M. Islam, N. Sadman, M. A. P. Mahmud, K. D. Gupta, and M. M. Ahsan, "A Review on Comparative Remarks, Performance Evaluation and Improvement Strategies of Quadrotor Controllers," *Technologies*, vol. 9, no. 2, p. 37, 2021. [Online]. Available: <https://www.mdpi.com/2227-7080/9/2/37>.
- [21] M. N. R. Shauqee, Parvathy & Mohd Suhadis, Nurulasikin. , "Quadrotor Controller Design Techniques and Applications Review," *INCAS BULLETIN*, 2021, doi: 10.13111/2066-8201.2021.13.3.15.
- [22] S. J. Andrew Zulu, "A Review of Control Algorithms for Autonomous Quadrotors," *Applied Sciences* 2014, doi: 10.4236/ojapps.2014.414053
- [23] A. A. a. R. Y. H. Shraim, "A survey on quadrotors: Configurations, modeling and identification, control, collision avoidance, fault diagnosis and tolerant control," *IEEE Aerospace and Electronic Systems Magazine*, vol. 33, pp. 14-33, 2018, doi: 10.1109/MAES.2018.160246.
- [24] C.-g. Kang, "Origin of Stability Analysis: "On Governors" by J.C. Maxwell," *IEEE Control Systems*, vol. 36, pp. 77-88, 2016.
- [25] J. D. Medaglia, "Clarifying cognitive control and the controllable connectome" *Wiley Interdiscip Rev Cogn Sci*, 2018, doi: 10.1002/wcs.1471.
- [26] P. R. K. Karl J. Åström, Control: A perspective *Control: A perspective*, vol. 50, no. 1, pp. 3-43, 2014, doi: <https://doi.org/10.1016/j.automatica.2013.10.012>.
- [27] S. N. C. H. B. Patel, "Developments in PID Controllers: Literature Survey," *International Journal of Engineering Innovation & Research*, vol. 1, no. 5, 2012.
- [28] J. M.-V. Ivan Lopez-Sanchez, "PID control of quadrotor UAVs: A survey *Annual Reviews in Control*, vol. 56, 2023, doi: <https://doi.org/10.1016/j.arcontrol.2023.100900>.
- [29] C. C. Z. R. S. K. R. S. K. S. Shanmugavel, "Development of a simple, low-cost autopilot system for multi-rotor UAVs" presented at the Conference: 2015 IEEE Recent Advances in Intelligent Computational Systems (RAICS), 2015.
- [30] J. H. Yuqing He, "Control Lyapunov Functions: New Framework for Nonlinear Controller Design" *IFAC Proceedings Volumes*, vol. 41, no. 2, pp. 14138-14143, 2008, doi: <https://doi.org/10.3182/20080706-5-KR-1001.02397>.
- [31] C.-I. S. Xue-ying Jiang , Ya-peng Xu , Kai Liu, Hui-yuan Shi & Ping Li "An adaptive backstepping sliding mode method for flight attitude of quadrotor UAVs" *J. Cent. South Univ*, vol. 25, pp. 616-631, 2018, doi: <https://doi.org/10.1007/s11771-018-3765-0>.

- [32] C. K. N. Parvathy Thampi M. S., "A Review On Controlling Techniques For Permanent Magnet Synchronous Motor (PMSM) And Current State Of The Art In The Research Area, *Communications on Applied Electronics*, vol. 7, pp. 8-17, 2019, doi: 10.5120/cae2019652808.
- [33] K. Ullah, J. Guzinski, and A. F. Mirza, "Critical Review on Robust Speed Control Techniques for Permanent Magnet Synchronous Motor (PMSM) Speed Regulation," *Energies*, vol. 15, no. 3, p. 1235, 2022. [Online]. Available: <https://www.mdpi.com/1996-1073/15/3/1235>.
- [34] B. M.-I. Morteza Nazari-Heris, "Application of Robust Optimization Method to Power System Problems" *Classical and Recent Aspects of Power System Optimization*, pp. 19-32, 2018, doi: <https://doi.org/10.1016/B978-0-12-812441-3.00002-1>.
- [35] A. M. S. Mostafavi, Mazaherifar, A., Mostafavi, S. UAV Placement and Trajectory Design Optimization: A Survey, *Wireless Personal Communications* pp. 2191–2210, 2022, doi: <https://doi.org/10.1007/s11277-021-09451-7>.
- [36] A. S. Amylia Ait Saadi, Yassine Meraihi, Asma Benmessaoud Gabis, Seyedali Mirjalili & Amar Ramdane-Cherif "UAV Path Planning Using Optimization Approaches: A Survey, *Archives of Computational Methods in Engineering* pp. 4233–4284, 2022, doi: <https://doi.org/10.1007/s11831-022-09742-7>.
- [37] M. Basharat, M. Naeem, Z. Qadir, and A. Anpalagan, "Resource optimization in UAV-assisted wireless networks—A comprehensive survey," *Transactions on Emerging Telecommunications Technologies*, vol. 33, no. 7, p. e4464, 2022, doi: <https://doi.org/10.1002/ett.4464>.
- [38] D. Wang, D. Tan, and L. Liu, "Particle swarm optimization algorithm: an overview," *Soft Computing*, vol. 22, no. 2, pp. 387-408, 2018/01/01 2018, doi: 10.1007/s00500-016-2474-6.
- [39] Q. G. Z. Zhao, "A kind of route planning method for UAV based on improved PSO algorithm," presented at the 2013 25th Chinese Control and Decision Conference (CCDC), Guiyang, China, 2013.
- [40] V. Ahuja and R. Hartfield, "Optimization of UAV Designs for Aerodynamic Performance Using Genetic Algorithms," in *51st AIAA/ASME/ASCE/AHS/ASC Structures, Structural Dynamics, and Materials Conference*.
- [41] M. T. a. G. L. V. Roberge, "Comparison of Parallel Genetic Algorithm and Particle Swarm Optimization for Real-Time UAV Path Planning,," *IEEE Transactions on Industrial Informatics*, vol. 9, pp. 132-141, 2013, doi: 10.1109/TII.2012.2198665.
- [42] E. L. C. Arroyo, "MODELING AND SIMULATION OF PERMANENT MAGNET SYNCHRONOUS MOTOR DRIVE SYSTEM," MASTER OF SCIENCE, ELECTRICAL ENGINEERING, UNIVERSITY OF PUERTO RICO MAYAGÜEZ CAMPUS, UNIVERSITY OF PUERTO RICO MAYAGÜEZ CAMPUS, 2006.
- [43] R. Umar, "Hybrid Cooperative Energy Detection Techniques in Cognitive Radio Networks. *IGI Global*, 2014.